The Company of **Biologists**

RESEARCH ARTICLE

Laser-mediated osteoblast ablation triggers a pro-osteogenic inflammatory response regulated by reactive oxygen species and glucocorticoid signaling in zebrafish

Karina Geurtzen[1,2,3], Alejandra Cristina López-Delgado[1,2], Ankita Duseja[1,2,4], Anastasia Kurzyukova[1,2,5] and Franziska Knopf[1,2,*]

ABSTRACT

In zebrafish, transgenic labeling approaches, robust regenerative responses and excellent *in vivo* imaging conditions enable precise characterization of immune cell behavior in response to injury. Here, we monitored osteoblast-immune cell interactions in bone, a tissue which is particularly difficult to *in vivo* image in tetrapod species. Ablation of individual osteoblasts leads to recruitment of neutrophils and macrophages in varying numbers, depending on the extent of the initial insult, and initiates generation of *cathepsin K+* osteoclasts from macrophages. Osteoblast ablation triggers the production of pro-inflammatory cytokines and reactive oxygen species, which are needed for successful macrophage recruitment. Excess glucocorticoid signaling as it occurs during the stress response inhibits macrophage recruitment, maximum speed and changes the macrophage phenotype. Although osteoblast loss is compensated for within a day by contribution of committed osteoblasts, macrophages continue to populate the region. Their presence is required for osteoblasts to fill the lesion site. Our model enables visualization of bone repair after microlesions at single-cell resolution and demonstrates a pro-osteogenic function of tissue-resident macrophages in non-mammalian vertebrates.

KEY WORDS: Osteoblast, Macrophage, Glucocorticoid, Reactive oxygen species, Lineage tracing, Zebrafish

INTRODUCTION

The skeleton and the immune system are close interaction partners, and crosstalk between both influences bone formation and regeneration (Takayanagi, 2007). Excessive activation of inflammatory cells causes bone destructive diseases such as rheumatoid arthritis, and long term treatment with anti-inflammatory steroids causes osteoporosis (Takayanagi, 2007). These diseases are associated with pain and

[1]Center for Regenerative Therapies TU Dresden (CRTD), Center for Molecular and Cellular Bioengineering (CMCB), TU Dresden, 01307 Dresden, Germany. [2]Center for Healthy Aging, Medical Faculty Carl Gustav Carus, TU Dresden, 01307 Dresden, Germany. [3]Laboratory of Clinical and Experimental Endocrinology, Department of Chronic Diseases, Metabolism and Ageing, KU Leuven, 3000 Leuven, Belgium. [4]Department of Oncology and Metabolism, Metabolic Bone Centre, Sorby Wing, Northern General Hospital, Sheffield S5 7AU, UK. [5]Faculty of Health and Medical Sciences, Biotech Research & Innovation Centre (BRIC), University of Copenhagen, 2200 Copenhagen, Denmark.

*Author for correspondence (franziska.knopf@tu-dresden.de)

A.C.L.-D., 0000-0003-2187-3938; F.K., 0000-0002-0420-7477

fragile bone, and represent major health issues, with strongly increasing incidence in the aging population (Odén et al., 2015).

After injury, recruitment of immune cells is the first step to ensure proper healing and to prevent the spread of inflammation (Duffield, 2003). Neutrophils dominate the early inflammatory response, becoming attracted to the respective sites, in order to clear debris and recruit macrophages (Kolaczkowska and Kubes, 2013). Early arriving macrophages display an inflammatory phenotype and release cytokines to induce tissue degradation and cell apoptosis (Leibovich and Ross, 1975; Diez-Roux and Lang, 1997). Resolution of inflammation during later tissue repair is promoted by anti-inflammatory macrophages (Novak and Koh, 2013). In mammalian fracture healing, macrophage contribution is essential for deposition and mineralization of bone matrix (Andrew et al., 1994). In particular, macrophages initiate bone remodeling by direct interaction with osteoblasts and osteoclasts in damaged bone (Batoon et al., 2017; Jilka et al., 2007). Moreover, macrophages produce osteoactive molecules which promote osteogenic differentiation and mineralization (Pettit et al., 2008; Sinder et al., 2015). Conversely, interaction with osteoblasts can induce cells of the monocyte/macrophage lineage to differentiate towards osteoclasts (Quinn et al., 1998).

Zebrafish has emerged as a powerful animal model to study immunity and inflammation (Trede et al., 2004; Renshaw et al., 2006; Hall et al., 2009; Niethammer et al., 2009), bone remodeling and skeletal disease (Witten and Huysseune, 2009; Kimmel et al., 2010; Hayes et al., 2013). Skeletal and immune cell biology are largely conserved among vertebrates, and zebrafish share the involved cell types, signaling pathways and molecules with mammals (Witten and Huysseune, 2009; Renshaw and Trede, 2012). Compared with classic vertebrate models such as rodents, zebrafish research benefits from early and rapid bone development in the presence of optical transparency up to a late larval stage (Cubbage and Mabee, 1996; Brittijn et al., 2009). *In vivo* imaging of immune and skeletal tissue can be performed using a variety of transgenic tools labeling specific bone and immune cell types, enabling the visualization of cellular interactions in real time (Chen and Zon, 2009; Hammond and Moro, 2012).

Studies investigating the cellular reaction of zebrafish bone cells to injury have focused on the adult fin, in particular after amputation (Knopf et al., 2011; Sousa et al., 2011; Singh et al., 2012; Ando et al., 2017), or on the zebrafish jaw (Paul et al., 2016; Ohgo et al., 2019). During fin and scale regeneration, live imaging of injury-responsive osteoblasts identified their ability to migrate and dedifferentiate, but also revealed the importance of *de novo* osteoblast generation (Geurtzen et al., 2014; Ando et al., 2017; Cox et al., 2018). Larval zebrafish models have been employed to understand vertebrate bone development (Kimmel et al., 2010; Sharif et al., 2014) and to decipher pathomechanisms underlying congenital skeletal disease (Fiedler

DEVELOPMENT

et al., 2018; Gistelinck et al., 2018; Tonelli et al., 2020). Although *in vivo* imaging studies on immune cell recruitment after infection and injury of non-osseous tissues (axonal tissue, mesenchymal fin fold tissue) are widely used (Ellett et al., 2011; Hasegawa et al., 2017; Isles et al., 2019; Li et al., 2012; Lieschke et al., 2001; Sanderson et al., 2015), sterile larval bone injury models are missing.

In this study, we present a novel laser-induced lesion paradigm in a developing skull bone in zebrafish, which provides a powerful tool to study the interaction between bone and immune cells *in vivo*. Using this model, we demonstrate the variable extent of immune cell recruitment in response to ablation of osteoblasts, illustrate the ablation-induced release of reactive oxygen species (ROS) and show that neutrophils, tissue-resident macrophages and *cathepsin K+* (*ctsK+*) osteoclast-like cells are attracted to dying osteoblasts, which are replenished by proliferation and migration of *osterix+* (also known as *sp7*) osteoblasts. Macrophage recruitment is inhibited by the systemic application of antioxidants as well as glucocorticoid (GC) administration, which in addition changes macrophage phenotype. Ablation of macrophages by a nitroreductase (NTR)-mediated approach leads to a reduction of osteoblasts at the lesion site. Our model can be used to elucidate the signals driving appropriate and disturbed macrophage and neutrophil recruitment to injured bone tissue *in vivo*, which is relevant for a variety of inflammatory bone diseases and for bone cell turnover during tissue homeostasis.

RESULTS

A 10% ablation of opercular osteoblasts is quickly reversed and leaves opercular growth unaffected

UV laser-mediated cell ablations, which lead to loss of fluorescent signal produced by transgenic fluorophore reporters

(Morsch et al., 2017), as well as two-photon-mediated ablations are known to effectively kill target cells in zebrafish (Mathias et al., 2006; Dehnisch Ellström et al., 2019). In order to create a confined lesion in bone and simulate osteoblast death, we performed osteoblast laser ablation in transgenic *osterix*:nGFP and *osterix*: nGFP×*histone*:mCherry zebrafish larvae at 6 days post fertilization (dpf), in which osteoblasts of the forming gill cover (opercle) are labeled by GFP and nuclei are labeled by histone-mCherry fusion protein (Knopf et al., 2011). We confirmed their ablation by the instantaneous disappearance of the fluorophores (Fig. S1A). Laser ablation led to the immediate fluorescence of the necrosis indicator ethidium bromide in the ablated area, suggesting cell rupture and release of the cell organelles and DNA (Fig. S1B). We evaluated the damage performed by laser ablation by quantifying the number of opercular osteoblasts with and without lesion at several time points. At 1 h post lesion (hpl) we detected a prominent loss of GFP signal at the lesion site (Fig. 1A), which corresponded to a loss of ~10% opercular osteoblasts (uninjured: $100\pm9.9\%$, control average=100%; lesioned: $87.4\pm10.2\%$ relative to 6 dpf unlesioned control; mean±s.d.; Fig. 1B). At 1 day post lesion (dpl), recovery of GFP fluorescence in the lesion site was observed, despite the fact that osteoblast numbers remained slightly (but not significantly) lower than in control fish (uninjured: $103.4\pm7.3\%$; lesioned: $93.5\pm10.1\%$). Complete recovery of osteoblast number was achieved at 2 dpl (uninjured: $110.9\pm10.6\%$; lesioned: $106.1\pm7.9\%$; Fig. 1B), illustrating the quick recovery of osteoblast numbers in laser-ablated opercles.

Next, we characterized the effect of laser-assisted osteoblast lesions on opercle structure and growth. To evaluate opercle volume, we stained zebrafish larvae by live Alizarin Red staining,
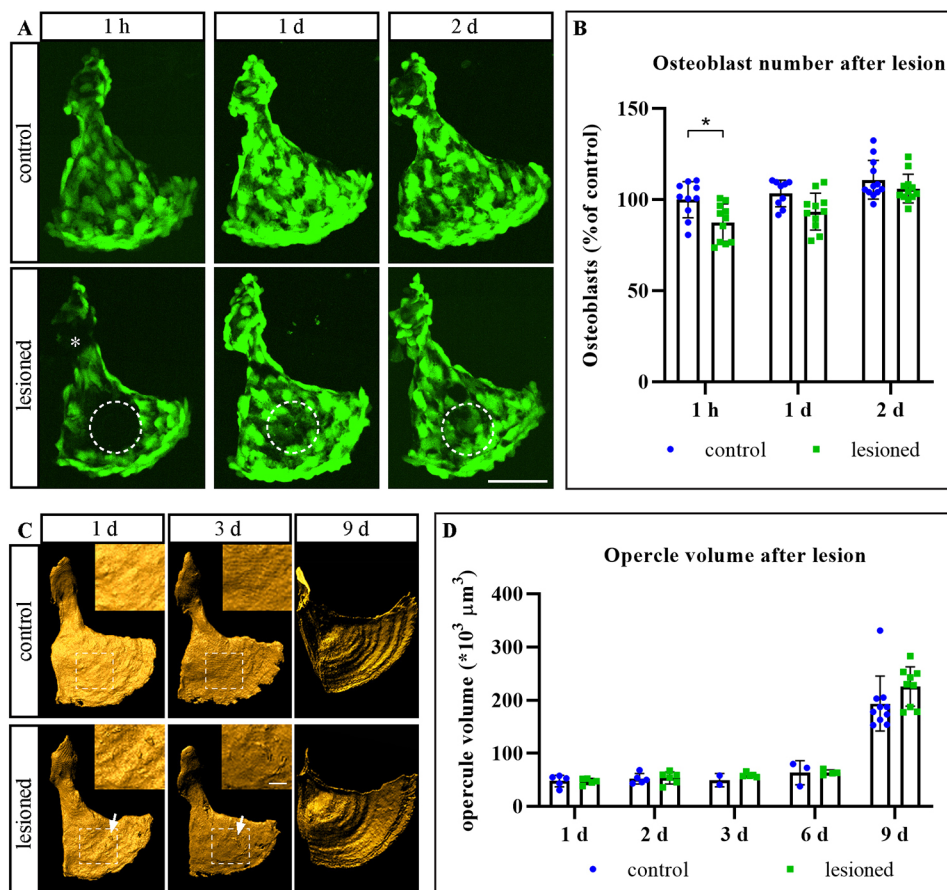

Fig. 1. Osteoblast recovery and opercular growth after ablation. (A) Representative images of the opercle region in transgenic *osterix*:nGFP 6 dpf larval zebrafish. White dashed line shows ablated area. (B) Quantification of osteoblast numbers from experiment shown in A in percent and normalized to the 6 dpf uninjured control. *n*=9-12. Data are mean±sd. *P=0.011 (Sidak's multiple comparison two-way ANOVA). (C) Opercles of 6 dpf lesioned and unlesioned control zebrafish stained with Alizarin Red. Insets show magnification of boxed areas: laser traces in the form of two spaced rings (arrows) and region without such marks in the control. (D) Quantification of opercular volume from experiment shown in C. *n*=3-10. Data are mean±s.d. (Sidak's multiple comparison two-way ANOVA). d, days; h, hours. Scale bars: 50 μm (A); 20 μm (C); 10 μm (C, insets).

which labels calcified structures (Javidan and Schilling, 2004), and rendered the surface with the help of IMARIS software. Ablation of osteoblasts led to a distinct structural change of the calcified matrix in the form of two closely spaced rings in places where the laser had hit (arrow and insets in Fig. 1C). These marks could be observed for several dpl, and disappeared by 9 dpl (Fig. 1C). As these marks were quite prominent, and because bone-forming osteoblasts were ablated, we wondered whether a change in opercle volume would result from lesion. Quantification of opercular volume across different stages showed that there were no significant differences between lesioned and respective control zebrafish larvae (uninjured versus lesioned, all ×10^3 μm^3: 1 dpl, 47.7±11.0 versus 47.0±5.6; 2 dpl, 52.08±9.9 versus 53.4±11.1; 3 dpl, 49.4±12.5 versus 58.9±4.1; 6 dpl, 63.3±22.4 versus 63.9±4.8; 9 dpl, 193.4±51.6 versus 225.4±37.2; Fig. 1D). This indicates that osteoblast ablation does not grossly affect opercular growth rate, although a temporal and spatially restricted structural damage in mineralized matrix could be observed due to the laser impact, and that osteoblast numbers recover quickly after ablation of a significant portion of osteoblasts.

Osteoblast number recovers by proliferation and migration of committed osterix+ osteoblasts

We wondered how the quick recovery of osteoblasts was accomplished. The most plausible explanation seemed to be the possibility that remaining osteoblasts proliferated in order to restore the necessary pool of osteoblasts. To test this, we injured transgenic zebrafish carrying the S/G2/M cell cycle phase reporter *EF1a*:mAG-zGem (Sugiyama et al., 2009) and found that a significant number of cells was labeled at 1 dpl (Fig. 2A,B). Next, we performed live imaging of transgenic *osterix*:nGFP zebrafish. Although osteoblast proliferation occurred (Movie 1), it was a rare event in time lapse movies (observed in 1 out of 15 larvae). At the same time, we observed slow relocation of pre-existing osteoblasts, as indicated by an increased number of osteoblasts reaching into the lesion site at 12 hpl (Fig. 2C). To confirm migration of pre-existing osteoblasts (or their progeny) into the ablation site, we performed CreERT2-loxP-mediated lineage tracing of *osterix*+ osteoblasts. *osterix*:CreERT2-p2a-mCherry×*hsp70*:R2nlsG double transgenic fish (Knopf et al., 2011) were either treated with 4-hydroxytamoxifen (4-OHT) to induce CreERT2 activity and excision of a loxP-flanked DsRed Stop cassette in osteoblasts or the vehicle control 1 day before lesion (Fig. 2D). At 3 dpl, the resulting nuclear GFP+ osteoblasts representing recombined cells and their progeny were visualized with the help of a heat shock (Fig. 2D,E) (Hans et al., 2009). In 4-OHT-treated larvae, GFP+ osteoblasts accumulated at the lesion site, whereas no GFP+ cells were detectable in the vehicle control (Fig. 2E). Comparison of 4-OHT-treated larvae with and without lesion showed that slightly more GFP+ osteoblasts can be detected when a lesion had been performed (70.24±13.34% in lesioned versus 61.22±16.26% in the uninjured control), although the difference was not statistically significant (Fig. 2F; Fig. S2). These results indicate that committed *osterix*+ opercular osteoblasts move into the ablation site to replenish the lost osteoblasts, a process which is supported by proliferation.

Osteoblast ablation leads to the release of immune cell attractants

Tissue damage and cell death lead to the release of a variety of chemokines and other cytokines, which have the potential to attract immune cells to the site of wounding (Duffield, 2003; Keightley et al., 2014). Both processes enhance the expression of extracellular

matrix (ECM) modifiers such as Matrix metalloproteinase 9 (Mmp9), a collagenase associated with inflammation in wounded zebrafish (LeBert et al., 2015). We made use of transgenic *mmp9*:EGFP zebrafish (Ando et al., 2017) to test whether Mmp9 expression is induced in zebrafish bone tissue upon osteoblast ablation. Although occasional GFP fluorescence was observed at 1 dpl, we detected robust induction of GFP at the lesion site at 2 dpl (uninjured versus lesioned: 1 hpl, 109.6±1.5 units versus 108.6±0.3 units; 1 dpl, 112.2±8.3 units versus 126.1±18.9 units; 2 dpl, 109.9±0.2 units versus 124.3±7.0 units; Fig. 3A,B). This expression may represent Mmp9 expression in resident cells surrounding the lesion or in recruited immune cells. We set out to identify earlier signs of inflammatory cues after osteoblast ablation and turned to ROS, which are known to be produced soon after acute wounding of other tissues such as the larval fin fold, where they are responsible for leukocyte attraction to the site of injury (Niethammer et al., 2009), or the tail (Romero et al., 2018). We pre-soaked *osterix*:nGFP larval zebrafish in CellROX orange dye, which starts to fluoresce upon ROS presence, performed lesions and concomitant *in vivo* imaging. Almost instantaneous activation of ROS-caused fluorescence was detected, and lasted throughout the imaging period of ∼20 min. Control larvae which had not been lesioned but equally soaked in the CellROX orange dye, did not show any signs of fluorescence (Fig. 3C; Movies 2 and 3). Similarly, osteoblast ablation via NTR in transgenic *osterix*:NTR-mCherry zebrafish (Singh et al., 2012) incubated with CellROX green led to ROS production (Fig. S3) (Kulkarni et al., 2018). These results indicate that sterile, laser-assisted ablation of a low number of bone-forming cells triggers a similar response to injury as seen in other, more severe, injury paradigms such as tissue resection. They also hint at a potential ability of the lesion paradigm to trigger recruitment of immune cells and osteoclasts (Callaway and Jiang, 2015), which, consequently, would allow the *in vivo* observation of leukocyte interactions with osteoblasts in bone tissue.

Neutrophils, inflammatory macrophages and osteoclast-like cells become recruited to the lesion site

Increased levels of *mmp9*:GFP expression and ROS after osteoblast ablation prompted us to test whether neutrophil numbers change upon lesion. Live imaging of double transgenic *osterix*:RFP×*mpo*:GFP zebrafish labeling osteoblasts and neutrophils revealed recruitment of neutrophils into the lesion area within minutes (Fig. 4A; Movie 4).

Next, we quantified the number of macrophages labeled by mCherry in double transgenic *osterix*:nGFP×*mpeg1*:mCherry zebrafish at different time points post lesion. Although absolute macrophage numbers in the head region posterior to the eye (Fig. S4A) did not change at 1 hpl, their number significantly increased until 1 dpl (uninjured versus lesion: 1 hpl, 24.6±4.8 cells versus 26.5±5.1 cells; 1 dpl, 25.3±5.2 cells versus 37.3±8.3 cells; Fig. 4B; Fig. S4A), which suggests recruitment of macrophages to the lesion site after neutrophil arrival. Likewise, we observed a recruitment of *mpeg1*+ macrophages in double transgenic zebrafish in which osteoblasts were ablated with the help of a two-photon laser (Fig. S4B). Live-imaging after ablation using the above double transgenic zebrafish confirmed fast recruitment of macrophages that had resided in the field of view (smaller than in Fig. S4A) into the osteoblast-ablated area, as well of slightly delayed recruitment of macrophages from outside the field of view starting at ∼20 min (Fig. 4C; Movie 5). More than 50% of macrophages passing the field of view during the imaging time were attracted into the lesion site during the first and second hpl (1 hpl, 50.8±9.0%; 2 hpl,

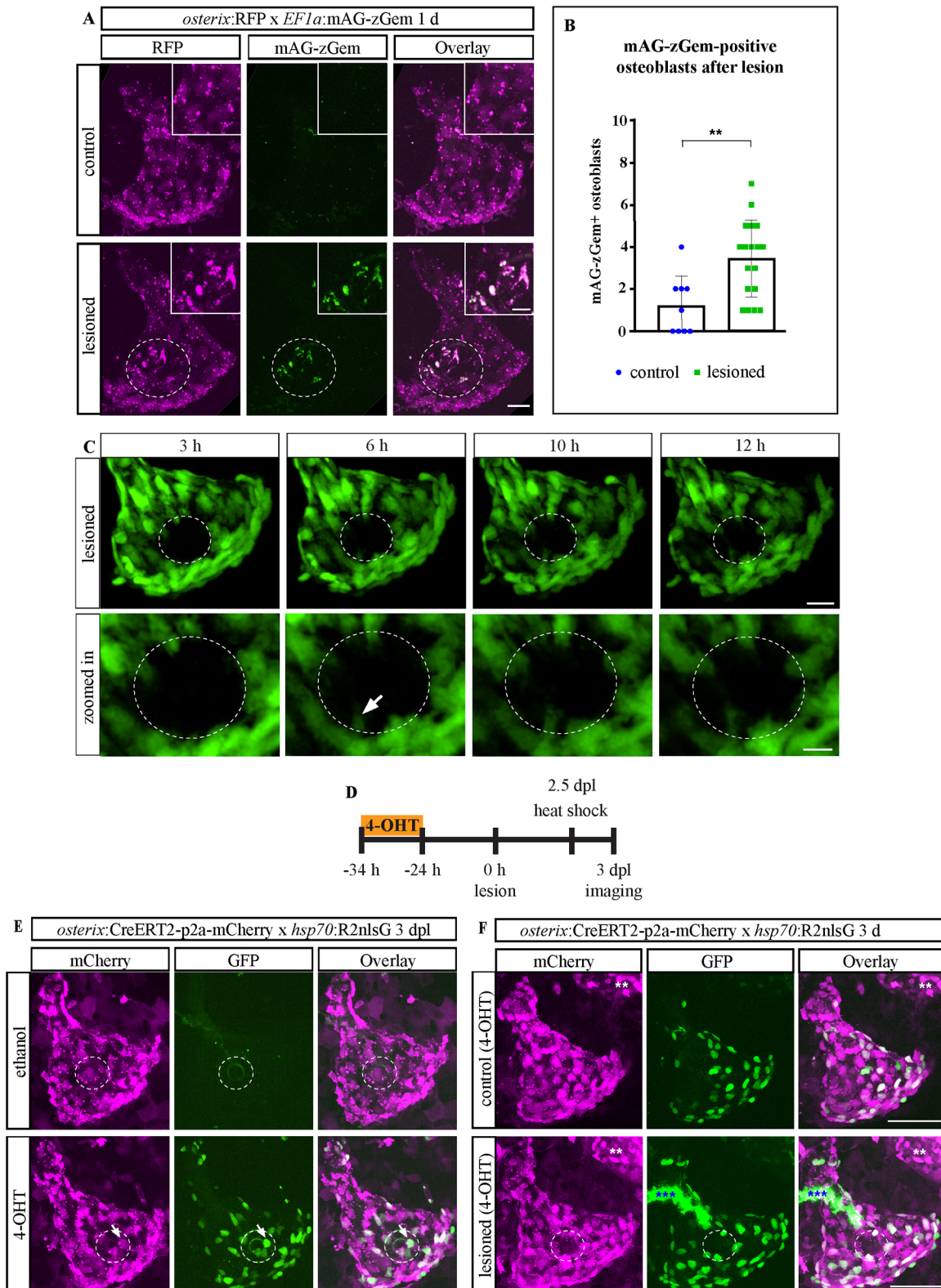**Fig. 2. Pre-existing *osterix*+ osteoblasts migrate into the lesion site.** (A) Representative images of *EF1a:mAG-zGem×osterix*:RFP zebrafish at 7 dpf, without lesion (control) and at 1 dpl. White dashed line shows area of lesion. Insets show target region. (B) Quantification of experiment shown in A. *n*=9-18. Data are mean±s.d. **P=0.0021 (unpaired two-tailed *t*-test with Welch's correction). (C) Images of opercular osteoblasts in 6 dpf transgenic *osterix*:nGFP larval zebrafish. Cellular extensions (arrow) reach into the lesion site within several hpl. *n*=3. (D) Scheme on CreERT2-loxP-mediated osteoblast lineage tracing approach. (E) Representative images of 4-OHT- and vehicle-treated *osterix*:CreERT2-p2a-mCherry×*hsp70*:R2nlsG zebrafish at 3 dpl (9 dpf). White arrow shows pre-existing committed osteoblasts located at the lesion site. *n*=5-7. (F) Representative images of 4-OHT-treated *osterix*:CreERT2-p2a-mCherry×*hsp70*:R2nlsG zebrafish at 9 dpf, without and with lesion performed at 6 dpf. White asterisks show dsRed signal ('R' in *hsp70*:R2nlsG zebrafish) in non-recombined, non-osteoblast cells. Blue asterisks in GFP channel show pigment cell. *n*=4-6. Scale bars: 20 µm (A,C); 10 µm (A,C, insets); 50 µm (E,F).
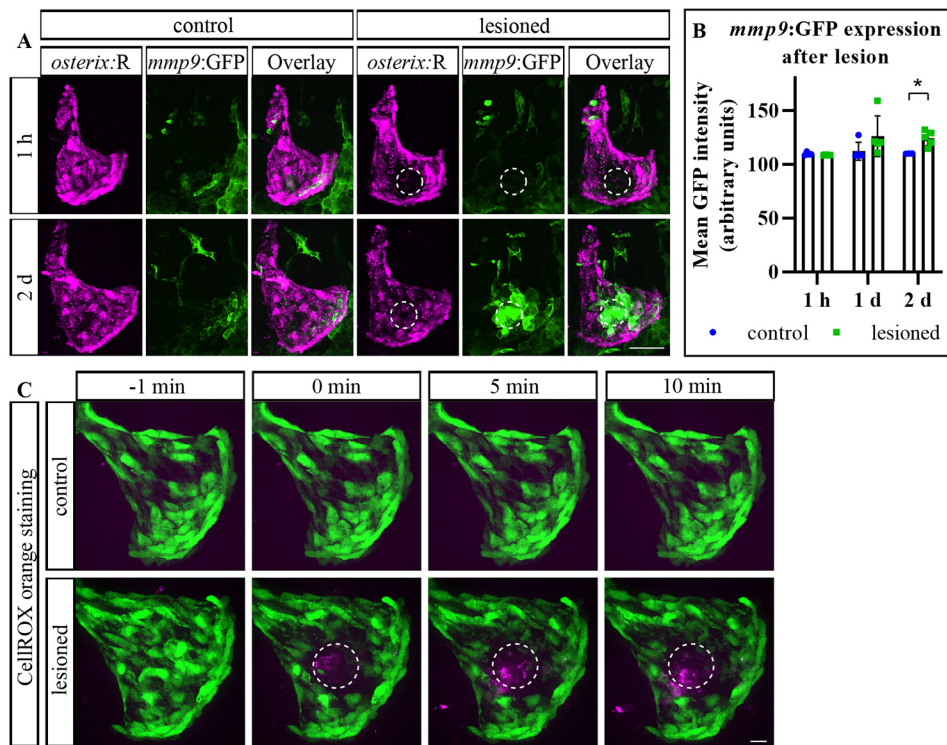
Fig. 3. Laser-assisted osteoblast ablation triggers Mmp9 production and ROS release. (A) Transgenic *osterix*:RFP×*mmp9*: GFP lesioned zebrafish showing *mmp9* activity at 2 dpl. (B) Quantification of experiment shown in A. *n*=3-5. Data are mean ±s.d. *P=0.010 (Welch's *t*-tests of pairwise comparisons of matching time points). (C) CellROX orange staining of lesioned and unlesioned transgenic *osterix*:nGFP zebrafish larvae. Green shows osteoblasts; magenta shows CellROX orange. *n*=6-7. White dashed line shows area of lesion. Scale bars: 50 μm (A); 10 μm (C).

68.0±7.4%; Fig. 4D). Live-imaging of *osterix*:nGFP×*mpeg1*: mCherry zebrafish combined with a transgenic marker for endothelial tissue, *kdrl*:CFP (Hess and Boehm, 2012), revealed that macrophages attracted to the lesion site arrive from within the tissues close to the lesion site and not from the blood stream, confirming their tissue-residency (Fig. 4E; Movie 6).

Early inflammatory responses are often associated with the inflammatory type of macrophages (Duffield, 2003), also in zebrafish (Nguyen-Chi et al., 2015). Using triple transgenic *osterix*:nGFP×*mpeg1*:mCherry×*irg1*:EGFP zebrafish larvae, in which activated macrophages (Sanderson et al., 2015) are labeled alongside osteoblasts, an increase in activated macrophages (mCherry/EGFP double+ migratory cells) was detected at 1 dpl [uninjured: 100.0±53.8% (normalized to all macrophages and to average of uninjured control); lesioned: 169.6±69.6%; white arrows in Fig. 5A,B]. Similarly, the use of *tnf-α*:EGFP×*mpeg1*: mCherry transgenic zebrafish (Marjoram et al., 2015) demonstrated increased numbers of inflammatory macrophages at 1 and 2 dpl (uninjured versus lesioned: 1 hpl, 6.0±2.9% versus 5.6±1.7%; 1 dpl, 9.4±5.5% versus 18.0±5.1%; 2 dpl: 14.8±6.3% versus 24.2±9.4%; white arrows in Fig. 5C,D). However, the majority of recruited macrophages at 1 and 2 dpl did not show the *tnf-α*+ inflammatory phenotype, which was only detected in about 20% of all macrophages (1 dpl: 18.0±5.1%; 2 dpl: 24.2±9.4%; Fig. 5D).

Next, we combined the macrophage reporter with an osteoclast reporter line established in our laboratory, in which *ctsK*+ cells are labeled by nuclear mCherry (*ctsK*:nlsmCherry; Fig. S5A). This approach enabled simultaneous observation of macrophages and osteoclast-like cells after lesion. Using triple transgenic *osterix*: nGFP×*mpeg1*:YFP×*ctsK*:nlsmCherry zebrafish we observed YFP/ nlsmCherry double positive migratory cells several hpl (white arrows in Fig. 5E). These cells were positive for *mpeg1* and *ctsK*, indicating that some macrophages convert to *ctsK*+ osteoclasts after osteoblast ablation. Accordingly, we detected significantly more

mpeg1/ctsK double positive cells at the lesion site compared with uninjured controls at 2 dpl (Fig. S5B,C).

These results demonstrate that ablation of approximately ten cells in a confined region is sufficient to recruit leukocytes, and that the rapid recruitment of neutrophils is followed by attraction of inflammatory macrophages. This indicates the presence of a classic early wound response in the sterile laser-assisted bone lesion paradigm. Potential conversion of macrophages into osteoclasts suggests macrophages as a source for osteoclasts in larval zebrafish.

Antioxidant treatment suppresses macrophage attraction to the lesion site

Macrophages are attracted to their sites of action by oxidized proteins, lipids and cellular debris of apoptotic cells which are either exposed to or produce high levels of ROS (Tan et al., 2016). The presence of ROS has also been shown to be imperative for wound repair in fin fold and tail resected zebrafish larvae (LeBert et al., 2015; Romero et al., 2018). In order to assess the importance of ROS for immune cell recruitment and osteoblast recovery after laser-assisted cell ablation in bone, we treated larval zebrafish with diphenyleneiodonium chloride (DPI), an NADPH oxidase inhibitor which efficiently blocks ROS directly after fin fold amputation (Fig. S6) (Robertson et al., 2016) and which does not impair macrophage and neutrophil number and motility (Movies 7 and 8). We then assessed the recruitment of macrophages to the osteoblast ablation site. We observed limited macrophage recruitment after DPI treatment (Fig. 6; Movie 9), which indicates that ROS production or release is essential for recruitment of macrophages to bone after lesion.

Immune-suppression by prednisolone alters macrophage recruitment to the lesion site

Steroids inhibit the inflammatory response and particularly suppress macrophage recruitment in a variety of mammalian models (Mosser and Edwards, 2008; Sharif et al., 2015; Cain and Cidlowski, 2017). Making use of a previously established regime of larval zebrafish
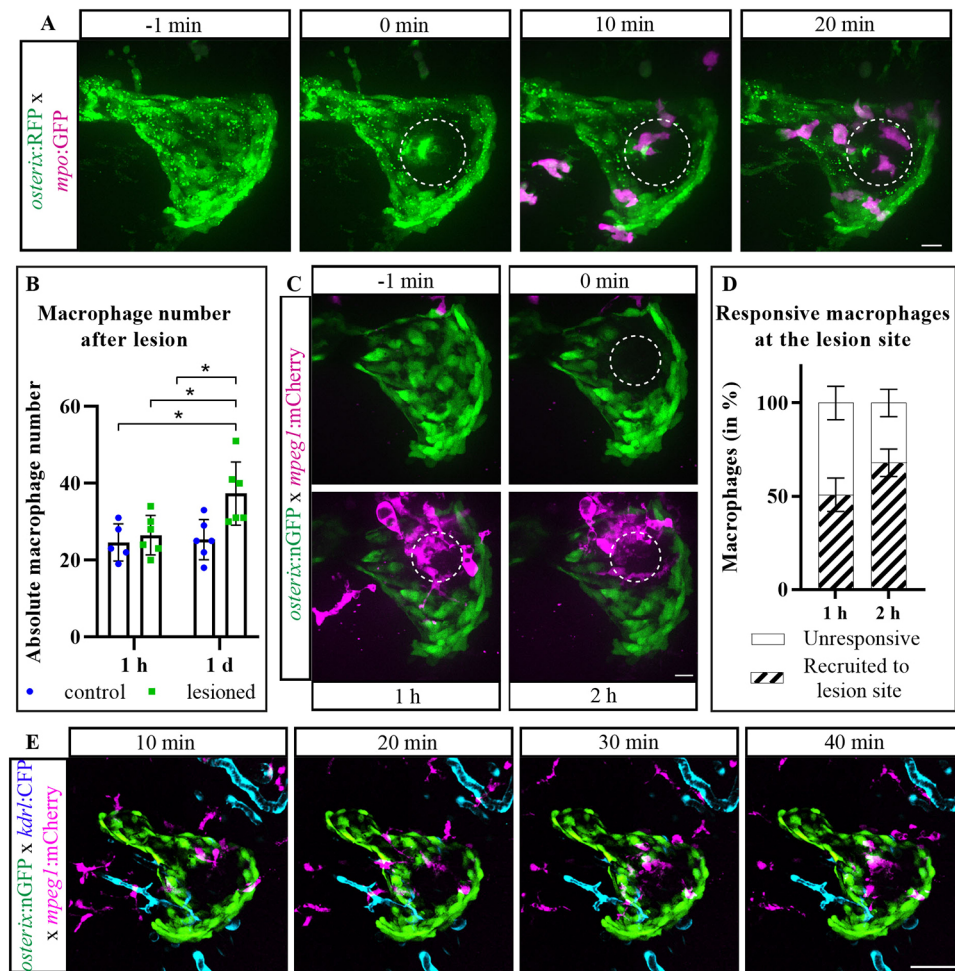
5

Fig. 4. Neutrophil and macrophage recruitment after ablation. (A) Time series of the opercle region in transgenic *osterix*:RFP×*mpo*:GFP zebrafish (RFP in green, GFP in magenta). Neutrophils show some autofluorescence in the RFP channel. *n*=7. White dashed line shows area of lesion. (B) Quantification of absolute macrophage number in the head region posterior to the eye (see Fig. S4A). *n*=5-6. Data are mean ±s.d. *P=0.014 (1 d control versus 1 d lesioned; Tukey's multiple comparison two-way ANOVA). (C) Time series of the opercle region of transgenic *osterix*:nGFP×*mpeg1*: mCherry zebrafish (mCherry in magenta). Separate experiment from that shown in B with smaller field of view. (D) Quantification of responsive macrophages migrating into the ablated area in the experiment shown in C. Unresponsive macrophages are found in the opercle area but not at the lesion site. *n*=5. Data are mean±s.e.m. Unpaired two-tailed *t*-test with Welch's correction. (E) Time series of the opercle region of transgenic *osterix*:nGFP×*kdrl*:CFP×*mpeg1*:mCherry zebrafish. *n*=3. Scale bars: 10 µm (A,C); 50 µm (E).

prednisolone treatment (Geurtzen et al., 2017), we tested whether mis-regulation of GC receptor-mediated signaling impacts (inflammatory) macrophage recruitment to the lesion site. After an 8 h pre-treatment with prednisolone, which did not significantly alter the number of macrophages in the entire head of 6 dpf larvae (DMSO: 119.4±10.7 cells; pred: 110.4±16.92; Fig. 7A), and subsequent lesion, accumulation of macrophages at the lesion site was strongly reduced (Fig. 7B; Movies 10 and 11). A mere 10% of the macrophages present in the opercle area were recruited into the lesion site during the first 2 hpl when prednisolone was administered, whereas more than 50% of nearby macrophages were recruited to the lesion site in vehicle-treated zebrafish (DMSO: 58.5±4.8%; pred: 12.8±7.2%; Fig. 7C).

We went on to test the impact of prednisolone on the appearance of *tnf-α*:EGFP+ inflammatory macrophages. Pre-treatment with the steroid significantly reduced inflammatory macrophage numbers as early as 1 hpl (DMSO versus pred, as percentage of all macrophages: 1 hpl, 19.1±8.8% versus 5.3±4.5%; 1 dpl, 29.8±9.1% versus 13.7±12.4%; Fig. 7D,E). These results show that GCs severely impair macrophage recruitment to microlesions in bone tissue, simultaneously suppressing their inflammatory activated phenotype.

Single-cell lesions allow the characterization of macrophage migratory features in response to osteoblast ablation and anti-inflammatory treatment

We asked ourselves whether smaller lesions of fewer osteoblasts would reliably attract leukocytes to the lesion site, a scenario

potentially relevant to homeostatic tissue conditions, in which loading and cell senescence may lead to isolated cell death (Kennedy et al., 2012). In order to investigate macrophage recruitment and migration in more detail and to further study the effects of excess GCs on these features, we performed ablation of two to three osteoblasts in the center of the opercle (Fig. 8A) and combined this with steroid drug administration. Recruitment of macrophages to the confined lesion site was apparent in both vehicle-treated and prednisolone-treated zebrafish (Fig. 8B; Movies 12 and 13); however, the relative contribution of nearby macrophages was strongly reduced compared with bigger lesions (big lesion: 58.5±4.8%; small lesion: 18.1±8.7%; both vehicle-treated). This indicates an injury-triggered dose-response-like mechanism in leukocyte recruitment. In prednisolone-exposed larvae, a mild decrease of macrophage recruitment was evident (DMSO: 18.1±8.7%; pred: 2.9±2.9%; Fig. 8C), similar to what was observed after ablation of a higher number of osteoblasts. This strongly suggests that death of individual bone cells is detected by locally patrolling macrophages in otherwise unaffected tissue, and that anti-inflammatory treatment affects immune cell-osteoblast communication during tissue homeostasis.

The lower number of recruited macrophages in microlesions enabled us to track individual macrophages by ARIVIS 4D software and to analyze migration characteristics in undisturbed, vehicle-treated zebrafish larvae versus individuals after GC treatment (Fig. 8D). Migratory track analysis revealed an average macrophage speed of 25.1±4.7 nm/s in control zebrafish, which was mildly but
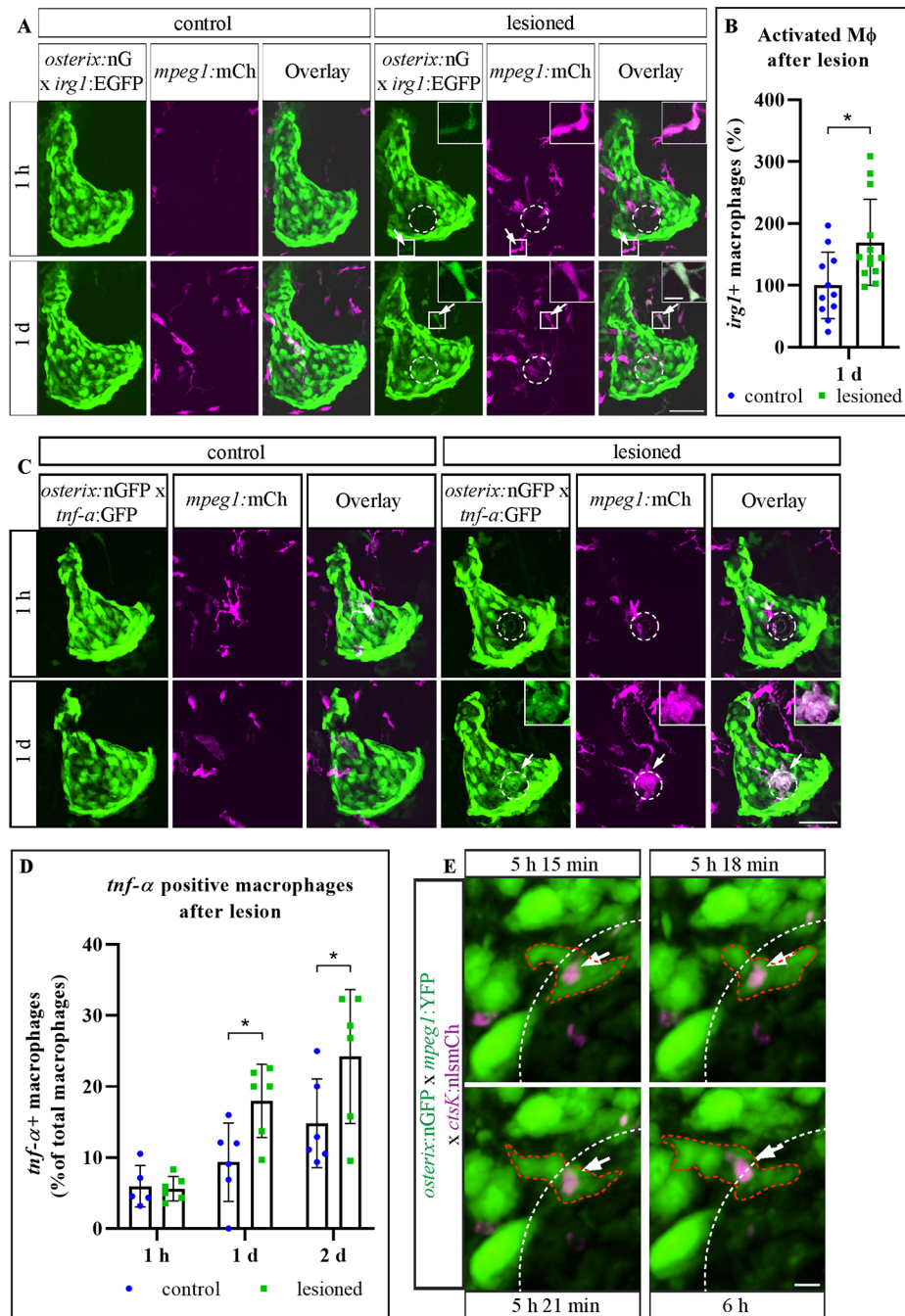
Fig. 5. Inflammatory macrophage and osteoclast presence after osteoblast ablation. (A) Representative images of transgenic *osterix*:nGFP×*irg*:EGFP×*mpeg1*:mCherry uninjured and ablated zebrafish opercular regions. Insets show magnification of boxed areas. (B) Quantification of activated macrophage numbers after osteoblast ablation in experiment shown in A. The relative number of *irg1*+ macrophages (as percentage of all macrophages and normalized to the uninjured control) is shown. Data are mean±s.d. *P=0.012 (unpaired two-tailed *t*-test with Welch's correction). MΦ, macrophage. n=11-13. (C) Representative images of transgenic *osterix*:nGFP×*tnf-α*:GFP×*mpeg1*:mCherry zebrafish opercular regions. Co-expression of *tnf-α*:GFP and *mpeg1*:mCherry is shown by arrows and in insets. (D) Quantification of inflammatory macrophages from experiment shown in C. The relative number of *tnf-a*+ macrophages (as percentage of all macrophages) is shown. n=5-6. Data are mean±s.d. 1 dpl *P=0.045; 2 dpl *P=0.026 (Sidak's multiple comparison two-way ANOVA). (E) Opercle region of transgenic *osterix*:nGFP×*mpeg1*:YFP×*ctsK*:nlsmCherry larvae at 5-6 hpl showing an *mpeg1*+, *ctsK*+ cell (white arrow and red dashed outline). n=4. White dashed line shows border of the lesioned area. Scale bars: 20 µm (A,C); 10 µm (insets A,C); 5 µm (E).

not significantly reduced to 16.8±2.5 nm/s by prednisolone treatment (Fig. 8E). Similarly, prednisolone exerted subtle (albeit insignificant) effects on macrophage straightness (DMSO: 0.13±0.02 units; pred: 0.09±0.01 units; Fig. 8F), a parameter describing directional migration of cells. Importantly, GC administration led to significantly reduced macrophage
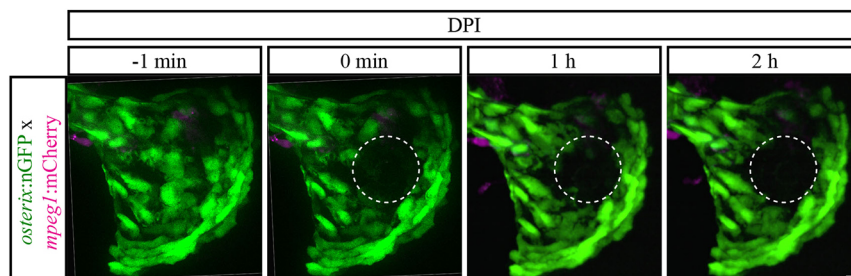

Fig. 6. Antioxidant treatment impairs macrophage recruitment to ablated osteoblasts. Time series of an osteoblast-ablated, transgenic *osterix*:nGFP×*mpeg1*:mCherry zebrafish treated with DPI for 5 h before lesion. Scale bar 10 µm. n=6. White dashed lines show border of the lesioned area.
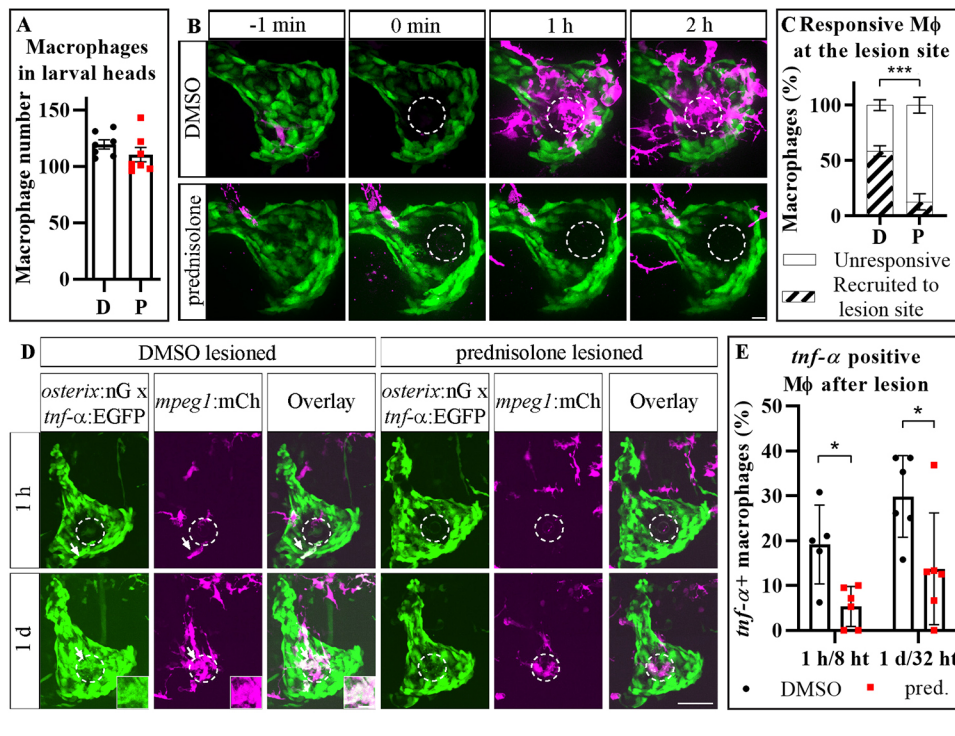
Fig. 7. Prednisolone treatment alters macrophage recruitment to the lesion site. (A) Quantification of the number of macrophages in the head of 6 dpf larval zebrafish after 8 h of treatment with prednisolone. *n*=7. Data are mean±s.e.m. Unpaired two-tailed *t*-test with Welch's correction. (B) Time series of the opercular areas of transgenic *osterix*:nGFP×*mpeg1*: mCherry prednisolone- and vehicle-treated larvae. (C) Quantification of experiment shown in B. *n*=6-7. Data are mean±s.e.m. ***P*=0.0003 (unpaired two-tailed *t*-test with Welch's correction). (D) Representative images of transgenic *osterix*:nGFP×*tnf-α*: GFP×*mpeg1*:mCherry osteoblast-ablated zebrafish opercular regions after prednisolone treatment. Arrows and insets show inflammatory macrophages co-expressing *tnf-α*:GFP and *mpeg1*: mCherry. White dashed line shows border of the lesioned area. (E) Quantification of experiment shown in D. *n*=5-6. Data are mean±s.d. 1 hpl, **P*=0.044; 1 dpl, **P*=0.013 (Sidak's multiple comparison two-way ANOVA). White dashed line shows border of the lesioned area. D, DMSO; MΦ, macrophage; P/pred., prednisolone. Scale bars: 10 μm (B, insets D); 20 μm (D).

maximum speed (Fig. 8G; DMSO: 216.4±32.29 nm/s; pred: 115.1±16.16 nm/s). This illustrates the agility of macrophages on their way to the microlesion site, and demonstrates the stationary phenotype of macrophages upon excess GC levels.

The lower number of macrophages attracted to the lesion site allowed a detailed investigation of macrophage morphology and respective changes upon lesion in GC-treated zebrafish. Macrophages displayed an amoeboid morphology (Fig. 8H, macrophage outlined in blue) or changed into an amoeboid phenotype while migrating towards the lesion site in control individuals (Fig. 8H, macrophage outlined in yellow). In contrast, macrophages had a ramified and elongated phenotype with several protrusions in prednisolone-exposed individuals (Fig. 8H, macrophage outlined in red). These results show that ablation of individual cells triggers a considerable immune response in zebrafish bone tissue, and that short-term GC treatment affects macrophage morphology and migration.

Macrophages support osteoblast recovery

As prednisolone treatment impaired macrophage recruitment to the ablation site and macrophages were recently suggested to promote osteoblast differentiation and bone mineralization in mammalian bone repair (Batoon et al., 2017), we investigated the effect of prednisolone administration on recovery of osteoblast numbers after lesion. We detected a significant reduction of osteoblasts in the opercle area after lesion of prednisolone-treated zebrafish (DMSO 104.7±8.43 cells versus pred. 92.3±6.62 cells; Fig. 9A), whereas the corresponding treatment did not have any effect in uninjured specimens (Fig. S7A,B). This indicated that macrophages may have a pro-osteogenic function in the repair of microlesions. To test this, we specifically ablated macrophages by a genetic NTR-mediated killing approach (Curado et al., 2008) in triple transgenic *osterix*:CreERT2-p2a-mCherry×*hsp70*:R2nlsG×*mpeg1*:YFP-NTR zebrafish (Petrie et al., 2014), and quantified the number of lineage-traced osteoblasts in the presence or absence of NTR [Fig. 9B; both groups treated with nifupirinol (NFP)]. Macrophage-ablated

samples showed a reduced number of lineage-traced, GFP+ osteoblasts at the lesion site (NTR− 2.73±0.90 versus NTR+ 1.58 ±0.90 cells; Fig. 9C,D). In a separate experiment testing the impact of macrophage presence on general bone growth, osteoblast numbers were significantly reduced after a longer ablation period (NTR− versus NTR+, both groups treated with NFP: 78.15±12.14 versus 69.30±6.24 cells; Fig. S7C).

In conclusion, manipulation of macrophage phenotype by pharmacologic GC treatment and their ablation by NTR affect osteoblast recovery after microscopic bone lesion.

DISCUSSION

In vivo and intravital imaging approaches in rodent species have progressed a lot in recent years (Peti-Peterdi et al., 2016; Yang et al., 2018; Kim and Bixel, 2020). A variety of studies examined the interaction of bone-producing cells with immune cells using *in vivo* microscopy (Kikuta et al., 2013; Hasegawa et al., 2019). Ishii and colleagues used two-photon confocal laser microscopy to observe osteoclast precursor migration to bone tissues in homeostatic conditions (Ishii et al., 2009). Similar approaches, some using bone explants, facilitated imaging of osteoblast–osteoclast interactions, osteoprogenitors during cranial bone defect repair and the mechanism of osteocyte embedding into bone ECM (Huang et al., 2015; Furuya et al., 2018; Shiflett et al., 2019; Dallas and Moore, 2020). Despite these advancements, limiting factors in terms of imaging depth persist for *in vivo* imaging of rodent bone tissue. Furthermore, the ability to resolve cellular dynamics in terms of cell shape changes, migratory behavior and cell-to-cell contacts remains challenging. This is also true for long-term imaging of rodent bone tissue *in vivo*, which, in contrast, can be performed up to several days in zebrafish larvae (Kaufmann et al., 2012).

Small teleost fish have proven extremely useful to monitor bone tissue during regeneration *in vivo* (Chatani et al., 2011; Cox et al., 2018; De Simone et al., 2021; Knopf et al., 2011; Phan et al., 2020b) and to observe immune cell behavior in response to soft tissue
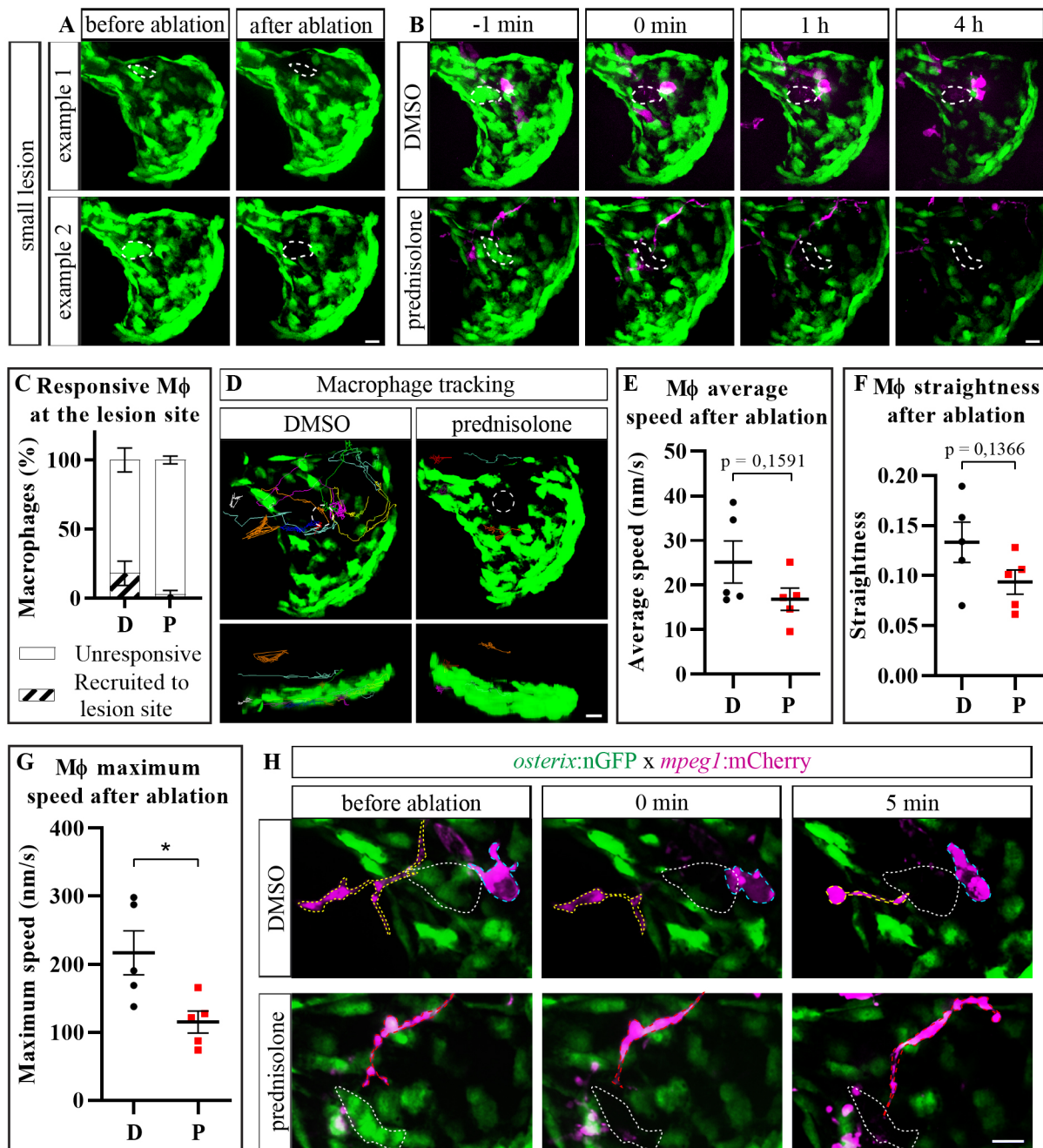
DEVELOPMENT

Fig. 8. Migratory features of macrophages in response to individual osteoblast ablation and prednisolone-treatment. (A) Examples showing ablation of a few isolated osteoblasts in vehicle-treated zebrafish (white dashed line shows precise region of osteoblast ablation). (B) Time series of the opercular region in transgenic *osterix*:nGFP×*mpeg1*:mCherry vehicle-treated (same as example 2 in A) versus prednisolone-treated larvae with a small lesion. (C) Quantification of the experiment shown in B (4 hpl). n=5. Data are mean±s.e.m. (unpaired two-tailed t-test with Welch's correction). (D) Representative images of individual macrophage tracking analysis in DMSO- and prednisolone-treated *osterix*:nGFP×*mpeg1*:mCherry larvae after small lesion. Arivis Vision 4D obtained tracks were overlaid with the first image after osteoblast ablation (upper panels x-y view, lower panels orthogonal view). (E) Quantification of average macrophage speed using tracking shown in D. n=5. (F) Quantification of macrophage straightness using tracking shown in D. n=5. (G) Quantification of the maximum macrophage speed using tracking shown in D. n=5. Data are mean±s.e.m. *P=0.032 (unpaired two-tailed t-test with Welch's correction). (H) Representative images of macrophages in the opercle region of *osterix*:nGFP×*mpeg1*:mCherry transgenic larvae treated with prednisolone or vehicle for 8 h. Time points shown: before, right after and 5 min post osteoblast ablation. White dashed line shows region of ablated osteoblasts; blue dashed line shows amoeboid macrophage; yellow dashed line shows macrophage changing from ramified to amoeboid phenotype; red dashed line shows ramified macrophage. D, DMSO; MΦ, macrophage; P, prednisolone. Scale bars: 10 μm.

injury (Gray et al., 2011; Li et al., 2012; Barros-Becker et al., 2017). Zebrafish lesion paradigms, mostly non-sterile, have been developed for several tissues, also to study immune cell responses *in vivo* (Nguyen-Chi et al., 2015; Ohnmacht et al., 2016; Renshaw et al., 2006). Many studies make use of larval fin fold resection ('tail fin amputation') (Demy et al., 2017; LeBert et al., 2015; Nguyen-Chi et al., 2017; Niethammer et al., 2009). The fin fold has a simple architecture, consisting of two epithelial layers innervated by sensory axons, comprises actinotrichia and interspersed mesenchyme, and lacks bone entirely (O'Brien et al., 2012).
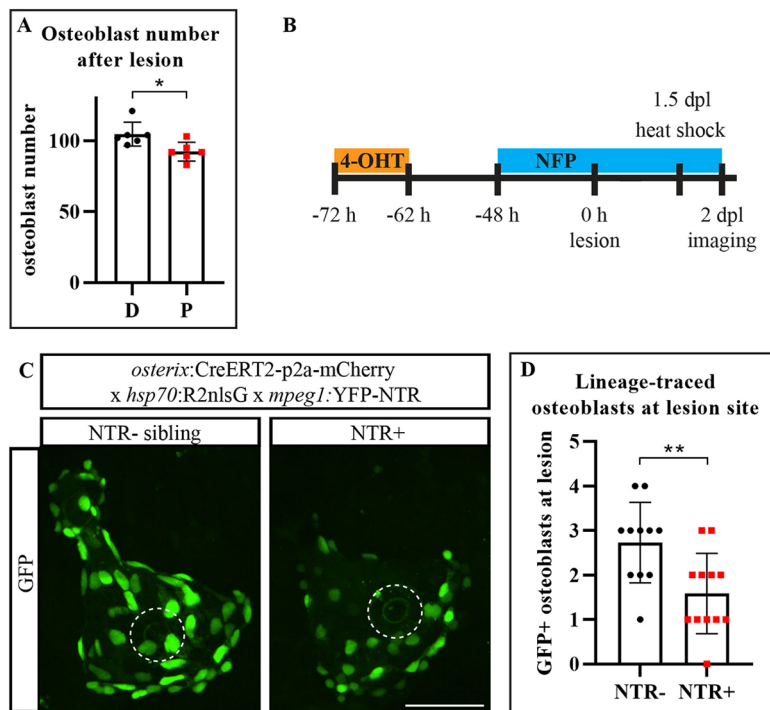
Fig. 9. Macrophage ablation affects osteoblast recovery.
(A) Quantification of absolute opercular osteoblast number in 7 dpf/1 dpl transgenic *osterix*:nGFP larval zebrafish after 1 day of prednisolone treatment. Data are mean±s.d. Unpaired two-tailed *t*-test with Welch's correction: *P=0.019. n=6. (B) Scheme on NTR mediated macrophage ablation combined with a CreERT2-loxP-mediated lineage tracing approach of osteoblasts. (C) Representative images of 4-OHT- and NFP-treated *osterix*: CreERT2-p2a-mCherry×*hsp70*:R2nlsG×*mpeg1*:YFP-NTR+ zebrafish and their NTR– siblings at 2 dpl. Both groups with NFP treatment. White dashed line shows border of lesioned area. (D) Quantification of experiment shown in C. *n*=11-12. Data are mean ±s.d. **P=0.006 (unpaired two-tailed *t*-test with Welch's correction). D, DMSO; P, prednisolone. Scale bar: 50 µm.

Here, we have established an approach to specifically ablate bone forming osteoblasts in larval zebrafish *in vivo*, which we used to evaluate the immune cell response towards this spatially confined, tissue-specific lesion. For our ablations, we predominantly used a UV laser cutter device designed to perform nanosurgery on cells and intracellular organelles (Colombelli et al., 2004). The loss of GFP and mCherry fluorescence was instantaneous and was accompanied by induction of a necrosis marker. We are therefore confident that osteoblasts were killed by our approach. However, we cannot exclude the possibility that ROS are also produced as a response to UV light in targeted osteoblasts or by nearby cells outside the focal plane (bleaching). Notably, two-photon laser ablation of osteoblasts elicited a similar immune cell response. Thus, our model represents a valuable tool to study the immune cell response after microscopic bone lesion and provides the possibility to evaluate the recruitment and behavior of immune cells in contributing to a balanced bone cell turnover and repair.

Recovery after cell loss is essential to ensure tissue health and the same applies to osteoblasts, the function of which is essential for maintenance and repair of the skeleton (Feng and McDonald, 2011). Many cell populations have shown the potential to generate osteoblasts, summarized under the term skeletal stem cells in mammals (Serowoky et al., 2020). In zebrafish, osteoblasts self-renew by dedifferentiation and proliferation of mature osteoblasts (Knopf et al., 2011; Sousa et al., 2011; Geurtzen et al., 2014), but also become recruited from progenitor cell pools (Ando et al., 2017; McDonald et al., 2021). Notably, proliferation of osteoblasts could be observed in response to laser-assisted osteoblast ablation, albeit not frequently. In addition to proliferation, stretching of cellular processes of pre-existing *osterix*+ osteoblasts towards the lesion site and lineage tracing of the same cells confirm contribution of committed osteoblasts. A potential alternative source of osteoblasts located at the lesion site may be cells that generate osteoblasts *de novo* from a precursor-like state, as seen in mammals, i.e. stromal cells or other cells reminiscent of mammalian skeletal stem cells, which needs to be tested in the future. A population of Smad9+

cells located at the anterior end of the opercle is a promising candidate. This cell population increases in size after NTR-mediated osteoblast ablation (Mcdonald et al., 2021). Despite this contribution, we have not detected a conspicuous size increase of this population (Fig. S8), and other potential contributors should be tested.

One important process after wounding is the production and release of cytokines attracting immune cells, which is essential to initiate tissue repair (Duffield, 2003). Mmp9, one of the signals induced after tissue damage (LeBert et al., 2015), triggers leukocyte migration (Purwar et al., 2008). Similarly, high ROS amounts are released after wounding (Yoo et al., 2012) and stimulate recruitment of immune cells in zebrafish (Niethammer et al., 2009; Feng et al., 2010). Sustained ROS levels are also observed after adult fin amputation, which includes the resection of bone (Gauron et al., 2013), and after resection of the larval notochord (Romero et al., 2018). Both *mmp9* activity and ROS production were induced by sterile laser-mediated osteoblast ablation, which illustrates that ablation of less than a dozen cells causes a wound response comparable to the one seen after non-sterile, more severe wounding. Although *mmp9* activity was visualized with the help of a transgenic reporter, making it difficult to infer whether Mmp9 release indeed plays a role in early leukocyte attraction, rapid ROS release was visualized real time, and treatment with the antioxidant DPI reduced leukocyte attraction, indicating that ROS are involved. Classic work on zebrafish fin fold resection (Niethammer et al., 2009) and tumor-transformed skin cells (Feng et al., 2010) demonstrated the importance of ROS-mediated immune cell attraction, which is likely to occur short-range (Jelcic et al., 2017). ROS blockage in our experiments may either cause reduced ROS levels at the ablation site or reduce ROS levels in macrophages, and therefore lead to impaired recruitment. Notably, ROS accumulate in macrophages and other leukocytes playing an important role in leukocyte polarization (Robinson, 2008; Tan et al., 2016). Moreover, ROS production plays a crucial role in bone homeostasis promoting osteoclastogenesis and bone resorption (Bai et al., 2005; Lee et al., 2005), and oxidative stress is strongly associated with bone

pathologies such as osteoporosis (Baek et al., 2010). To our knowledge ROS have not been visualized at cellular resolution *in vivo* in bone before, making this the first study to successfully label ROS release after osteoblast ablation in a living organism. It remains unclear whether increase of ROS in or by individual osteoblasts is sufficient to attract immune cells. In the future, tools such as KillerRed will enable tissue and cell type specific generation of ROS (Teh et al., 2010; Formella et al., 2018) in the growing opercle without cell ablation. This will lead to the further characterization of the impact of ROS on bone cell turnover and tissue homeostasis.

Tissue damage leads to a rapid and essential immune cell influx. In our assay, neutrophils were recruited first and macrophages followed shortly after, which is in agreement with previous work (Kolaczkowska and Kubes, 2013; Keightley et al., 2014). The early responding macrophages were tissue-resident, and might be responsible for later recruitment of monocyte-derived macrophages (Davies et al., 2013). The average macrophage speed was comparable with previously reported data (Barros-Becker et al., 2017; Ellett et al., 2011; Li et al., 2012). Acquisition of *ctsK* expression in some macrophages was observed, indicating osteoclast differentiation. In medaka, a similar process was observed after RANKL (Receptor activator of NF-κB ligand) overexpression (Phan et al., 2020a,b). Some caution is warranted, as *ctsK* also labels mesenchymal cells in some tissues (Debnath et al., 2018) and we observed immobile *ctsk*:nlsmCherry+ nuclei at a distance from the opercle, in locations unlikely to contain osteoclasts (see e.g. Fig S5A). It is noteworthy that conversion of macrophages to osteoclasts depends on inflammatory signals such as Tnf-α (Phan et al., 2020a). We detected increased expression of *tnf-α* in some macrophages recruited to the lesion site, and these cells are good candidates for differentiation into osteoclasts. Further investigation of additional osteoclast-specific and inflammatory markers, such as tartrate-resistant acid phosphatase, will reveal the importance of macrophage recruitment and inflammatory phenotype for osteoclastogenesis at the lesion site.

Macrophage contribution to wound healing is dependent on the subtype characteristics. In zebrafish, transgenic reporter lines enable investigation of macrophage phenotypes throughout inflammation and its resolution (Ellett et al., 2011; Gray et al., 2011; Walton et al., 2015). Available tools showed that, similar to the mammalian situation, two waves of macrophages (inflammatory and regenerative) emerge in soft zebrafish tissues after resection (Nguyen-Chi et al., 2017).

In this work, we evaluated the amount of activated and inflammatory macrophages at relatively early time points post cell ablation. Increased *irg1*:GFP+ macrophages were already detected at 1 hpl, indicating that these activated macrophages respond fast. Irg1 (Acod1) labels activated macrophages and it is often expressed by pro-inflammatory macrophages (Sanderson et al., 2015). We therefore suggest that activated macrophages populate the lesion site early on and become polarized towards the inflammatory phenotype. On the basis of *tnf-α*:GFP expression, about 20% of macrophages in the opercle area and at the lesion site were identified as inflammatory macrophages at 1 dpl. In fin fold-resected zebrafish ~30% of inflammatory macrophages were reported at 24 h post amputation, and more inflammatory macrophages could be detected earlier (Nguyen-Chi et al., 2017). In the future, laser-assisted osteoblast ablation will allow further studies of the kinetics of the inflammatory response to damage in bone tissue, in particular with respect to normal and dysregulated resolution of inflammation.

Tight regulation of the immune response is essential for tissue repair, and overexerted actions can be harmful. In the bone microenvironment, a variety of inflammatory conditions and therapy-associated diseases such as rheumatoid arthritis and GC-induced osteoporosis affect bone health (den Uyl et al., 2011; Feng and McDonald, 2011). In order to develop novel therapies for such diseases and to counteract adverse effects of immunosuppressive treatment, it is crucial to precisely understand how immune cells are affected in these conditions. Zebrafish fin fold regeneration models combined with high-dose GC treatment (Hall et al., 2014; Sharif et al., 2015; Chatzopoulou et al., 2016) showed that GCs suppress the attraction of macrophages and neutrophils and impair tissue regeneration. Here, we investigated the effect of GCs on immune cells *in vivo* in the context of bone cell turnover and microscopic bone repair. In particular inflammatory macrophages were affected by GC exposure, as reported previously (Cain and Cidlowski, 2017; Russo-Marie, 1992; Xie et al., 2019). Morphology, which can be used as a readout for activation and polarization status of macrophages (McWhorter et al., 2013), was altered after GC exposure. Inflammatory, activated macrophages display an amoeboid morphology with few dendrites whereas anti-inflammatory macrophages are more elongated and display more dendrites, also in zebrafish (Nguyen-Chi et al., 2015). GC exposure impaired the activated, amoeboid morphology of macrophages in our model. Consistently, *tnf-α*:GFP+ macrophage numbers dropped in GC-treated zebrafish, similar to effects after fin fold resection and concomitant treatment (Nguyen-Chi et al., 2015).

Contrasting data have been obtained concerning the effect of GCs on immune cell migration, also varying depending on the GC used. Whereas beclomethasone leaves macrophage migration unaffected in fin fold resected zebrafish (Chatzopoulou et al., 2016; Xie et al., 2019), high dose dexamethasone treatment reduces macrophage recruitment in the same model (Sharif et al., 2015). Here, we used prednisolone, a third synthetic GC, to test for its immunosuppressive effects after individual osteoblast ablation. Treatment led to a reduced macrophage migratory ability in terms of maximum speed and recruited macrophage number. This is in agreement with previous results on adult bony fin ray-amputated zebrafish, in which prednisolone treatment led to impaired macrophage accumulation in fin regenerates (Geurtzen et al., 2017).

High dose GCs are known to strongly affect osteoblasts by inducing osteoblast apoptosis while impairing osteoblast proliferation and maturation (den Uyl et al., 2011; Weinstein, 2012). To date, it is unclear whether these anti-osteogenic effects are exclusively mediated directly or whether alteration of macrophage number and phenotype contribute to these effects. During mammalian bone repair, macrophages promote osteoblast differentiation and bone mineralization (Pettit et al., 2008), in particular after fracture (Batoon et al., 2017). In our lesion model, macrophage ablation led to reduced osteoblast numbers at the lesion site, reflecting either impaired proliferation or migration of *osterix*+ osteoblasts. Decreased osteoblast numbers in the developing opercle after macrophage ablation point to a similar compromising effect, which was also observed in fractured mouse bones after tissue-resident macrophage ablation (Alexander et al., 2011; Batoon et al., 2017). This illustrates the capacity of tissue-resident macrophages to support bone formation in mammalian and non-mammalian vertebrates. In the future, it will be interesting to test osteoblast- and macrophage-specific knockout tools in zebrafish, e.g. to delete the GC receptor *nr3c1*, or to target prednisolone to phagocytic macrophages specifically, in order to decipher the indirect negative impact of GC exposure on osteoblasts via immune cells. Moreover, it will be interesting to compare anti-migratory effects of different synthetic GCs on macrophages and neutrophils across different wounding assays and tissues, specifically when taking bone tissue into account.

DEVELOPMENT

Our model represents a novel approach to study bone cell turnover in homeostasis and repair. We show that ablation of only few osteoblasts is sufficient to initiate an immune cell response of graded severity, depending on how many cells were ablated initially. This is especially interesting considering that osteoblast senescence and cell death are frequent processes in bone homeostasis, with osteoblasts having a relatively short life span (Manolagas, 2000). The consequences of isolated osteoblast death during homeostasis and medical treatment, as well as their replacement, are not particularly clear. One aspect of osteoblast biology is their declined performance in aged bone, which is partly mediated by accumulation of ROS (Kim et al., 2018), and rising levels of GCs (Almeida and O'Brien, 2013). Both factors, which we modeled with the help of laser-assisted osteoblast ablation, influence bone health directly and indirectly, by impairing osteo-immune cell communication (Ahmad et al., 2019; Lean et al., 2005). Although we are aware that the presented assay makes use of a growing bone of simple structure, we suggest to use it to *in vivo* monitor the processes of osteoblast recovery after damage, and to study the varying contribution of immune cells to bone repair and integrity. In addition, interaction of leukocyte cell types, such as the process of reverse migration of neutrophils first observed in zebrafish (Mathias et al., 2006) and later demonstrated in mammals (Woodfin et al., 2011), and the generation of macrophage/monocyte-derived osteoclasts in response to ROS and increased stress signaling can be studied. Finally, the model enables studies on the contribution of different osteoblast progenitor cell pools to osteoblast recovery and can potentially be used in slightly older animals to visualize the plasticity of mature osteoblasts undergoing dedifferentiation.

MATERIALS AND METHODS
Animal experiments
All procedures were performed in accordance with the animal handling and research regulations of the Landesdirektion Sachsen (permit numbers AZ DD25-5131/354/87, DD25-5131/450/4, 25-5131/496/56 and amendments).

Fish lines and husbandry
The following previously described transgenic zebrafish lines were used: osterix:nGFP [Tg(*Ola.Sp7*:NLS-GFP)[zf132]] and osterix:RFP [Tg(*Ola.Sp7*:mCherry)[zf131]] (Spoorendonk et al., 2008), histone Cherry [Tg(*h2afv*:h2afv-mCherry)[tud7]] (Knopf et al., 2011), mmp9:EGFP [TgBAC(*mmp9*:EGFP-NTR)[tyt206]] (Ando et al., 2017), mpo:GFP [Tg(BAC*mpo*:gfp)[i114]] (Renshaw et al., 2006), mpeg1:mCherry [Tg(*mpeg1*:mCherry)[gl23]] (Ellett et al., 2011), mpeg1:YFP-NTR [Tg(*mpeg1*:NTR-EYFP)[w202]] (Petrie et al., 2014), tnfa:GFP [TgBAC(*tnfa*:GFP)[pd1028]] (Marjoram et al., 2015), irg1:EGFP [Tg(*acod1*:EGFP)[nz26]] (Sanderson et al., 2015), osterix:CreERT2-p2a-mCherry [Tg(*Ola.sp7*:CreERT2-P2A-mCherry)[tud8]] (Knopf et al., 2011), hsp70:R2nlsG [Tg(*hsp70l*:loxP-DsRed2-loxP-nlsEGFP)[tud9]] (Knopf et al., 2011), kdrl:CFP [Tg(*kdrl*:CFP)[zf410]] (Hess and Boehm, 2012), *EF1a*:mAG-zGem [Tg(*EF1a*:mAG-zGem(1/100))[rw0410h]] (Sugiyama et al., 2009) and osterix:NTR-mCherry [Tg(*Ola.Sp7*:mCherry-Eco.NfsB)[pd46]] (Singh et al., 2012).

For creation of the *ctsK*:nlsmCherry transgenic zebrafish line [Tg(*ctsK*:nlsmCherry)[tud301]] a fragment containing the 4 kb promotor region and start of exon1 of the *Danio rerio ctsK* was cloned upstream of nlsmCherry into a pBluescript-based vector containing Tol2 transposable sites flanking the insert (vector kindly provided by Anke Weber and Stefan Hans, CRTD, Dresden, Germany). The following primers were used for amplification: ATATCCTCTCACAGGACATCAAACAGCGAAACGAG (adding an EcoNI restriction site) and TATAGGCCGGCCTGAGCAAGAA-GAAATGCACC (adding an FseI restriction site). EcoNI and FseI restriction enzymes were used for cloning. A transgenic line was created by injecting the plasmid DNA with transposase mRNA into fertilized eggs. Throughout larval growth transgene expression was detectable in the

pharyngeal region comparable with another previously published zebrafish *ctsK*-line (Sharif et al., 2014). Fish were bred and maintained as previously described (Brand et al., 2002).

Lesion paradigm and *in vivo* imaging
In order to perform osteoblast ablations, zebrafish larvae were anesthetized in 0.02% Tricaine (MS222, Merck) and embedded in 1% low melt agarose (LMA, Biozym Scientific) in E3 in a glass-bottom microwell dish (35 mm, 14 mm microwell, MatTek Corporation). To immobilize the larvae, 20 µl of 0.4% Tricaine was added to 1.5 ml LMA (final concentration 0.005% Tricaine). They were laid on the side to position the opercle region close to the glass bottom for imaging accessibility. For prednisolone treatment the larvae were kept in prednisolone (Merck) or DMSO (Merck) control conditions by adding autoclaved E3 with 0.01% Tricaine and 25 µM prednisolone or 0.05% DMSO to the dish after the LMA had solidified, otherwise E3 with 0.01% Tricaine was added. The osteoblast lesion was performed using an Andor spinning disk system consisting of a Zeiss AxioObserver.Z1 equipped with a Yokogawa CSU-X1, a custom built laser ablation system with a pulsed UV Nd:YAG laser (JDS Uniphase Power Chip), and an iXon+ camera facilitating simultaneous imaging with LabVIEW 2009. The system was designed and built to perform laser nanodissection and intracellular nanosurgery (Colombelli et al., 2004). The wavelength of the laser is 355 nm, transmission at 355 nm is 92%, the energy per pulse is 10 µJ, the pulse width is 500 ps with a repetition rate of 1 kHz. The same laser cutter settings were used throughout the study, consisting of 2.0 intensity, 20 pulses/shot, four shots/µm^2 and two shooting circles of 15 and 7 µm Ø. Successful ablation was confirmed by loss of GFP signal and mCherry signal, respectively. Two-photon ablations were performed with an inverse laser scanning Leica SP8 FALCON microscope (tunable Spectra-Physics Insight X3 multiphoton laser at 800 nm for 10 s, 50% laser power, scan speed 400 MHz, VISIR 25×/0.95 water objective, area of 25 µm diameter). Afterwards the larvae were carefully removed from the LMA and kept in E3 until further imaging was performed. Non-lesioned controls were mock-treated i.e. they were also anesthetized and embedded in LMA. In some experiments, imaging of ablated and uninjured larvae was performed with the help of a Zeiss LSM 980 confocal microscope and a Leica SP5 laser scanning microscope, respectively.

Short-term imaging was performed with LabVIEW 2009 with the setup described above and long term imaging was performed with Andor iQ2 software or a Dragonfly spinning disk equipped with a sCMOS camera and Fusion software. In both imaging approaches, the same laser power, gain settings and exposure times were used. Larvae were kept in LMA after the lesion and were continuously imaged at different time intervals. Data were processed with ImageJ Software version 1.53c or Arivis Vision4D version 2.12.6 and 3.3.0 where mentioned, in order to obtain images and movies. Arivis Vision4D version 2.12.6 was used to track macrophages. First, the data were filtered using a convolution enhancement filter which was followed by drift correction using the GFP channel. Afterwards, individual macrophages were tracked using the blob finder and Brownian motion segment tracker. Only macrophages with complete cell bodies visible and which were very present in the field of view for more than 30 min were tracked. At the end, the tracking was manually verified, aberrant tracks were excluded and separated tracks were merged.

Drug treatments
Prednisolone treatment of zebrafish larvae was carried out as previously described (Geurtzen et al., 2017). Treatment started at 6 dpf (8 h before ablation) and lasted for up to 32 h in total.

DPI (Merck) treatment of 3 dpf zebrafish larvae before fin fold resection was carried out as previously described (Robertson et al., 2016). DPI treatment on 6 dpf larvae started 5 h before laser ablation and continued throughout the live imaging period with the same concentration used on 3 dpf larvae (100 µM). To test for the influence of DPI on general macrophage and neutrophil motility, 5 dpf larvae without ablation were used.

NFP (Sigma-Aldrich, #32439) treatment was performed as previously described (Bergemann et al., 2018). A 2.5 mM stock solution of NFP in DMSO was prepared and stored at −20°C. Larval zebrafish were soaked in

2.5 μM NFP for up to six consecutive days to ablate macrophages in the dark at 28°C. Osteoblast ablation was performed for either 4-7 h or a day starting at 4 dpf.

Fin fold resection
For fin fold resection, 3 dpf larvae were anesthetized and fin fold resection was performed as previously described (Isles et al., 2019).

Staining techniques
Alizarin Red staining of the live zebrafish larvae was performed as previously described (Kimmel et al., 2010). For quantification of the opercle volume the surface tool in Imaris 8.1 was used to reproduce the Alizarin Red stained area surface and to calculate the corresponding volume.

CellROX staining was conducted as previously described (Kulkarni et al., 2018). Both CellROX green and CellROX orange (Thermo Fisher Scientific) were used. After staining, larvae were embedded in 1% LMA, lesioned and live imaged for 15 min in the case of laser ablation.

Necrosis staining was performed as previously described (Roger et al., 1996) with modifications. In brief, live 6 dpf larvae were incubated for 30 min in 2 μg/ml ethidium bromide (Roth). Ethidium bromide is taken up when cytoplasmic membrane integrity is lost (Renvoizé et al., 1998). Larvae were washed twice for 20 min in PBS, and embedded in 1% LMA. Larvae were imaged in an SP8 confocal microscope before and immediately after ablation. To detect ethidium bromide signal, samples were excited with 520 nm laser wavelength.

Immunohistochemical staining was performed as follows: larvae were rehydrated after fixation with 4% PFA and stored in methanol using a methanol-PBS series including Triton X (5 min 75% methanol in PBS, 5 min in 50% methanol in PBS, 5 min in 25% methanol in PBS, two quick washes in 0.2% PBS Triton X, 3×30 min 0.2% PBS Triton X), and further permeabilized for 90 min with proteinase K (15 μg/ml, Roche). Specimens were blocked in blocking solution (5% normal goat serum+5 mg/ml bovine serum albumin in 0.2% PBS Triton X) for 2-5 h and then incubated in primary antibodies (chicken-anti-GFP, 1:2000, #ab13970, Abcam; rabbit-anti-Smad9, 1: 200, #ab96698, Abcam; in blocking solution) overnight at 4°C with gentle agitation. The next day, they were washed briefly twice with 0.2% PBS Triton X, followed by 1 h of washes with 0.2% PBS Triton X (6× for 10 min). Samples were blocked again with blocking solution and the secondary antibodies (anti-chicken-Alexa488, #A11039, and anti-rabbit-Alexa555, #A21428, at 1:500, both Thermo Fisher Scientific) were incubated overnight at 4°C in blocking solution. Afterwards, samples were washed briefly twice with 0.2% PBS Triton X, followed by 1 h of washes with 0.2% PBS Triton X (6× for 10 min), and prepared for imaging.

Osteoblast fate mapping
osterix:CreERT2-p2a-mCherry, *hsp70*:R2nlsG double transgenic 5 dpf larvae were soaked in 10 μM 4-OHT (Merck) or the corresponding amount of vehicle control ethanol for 10 h. Larvae were lesioned at 6 dpf. One or two days later (7 or 8 dpf), larvae were heat shocked once at 37°C for 1 h. Roughly 12 h post heat shock the larvae were analyzed for recombination by the appearance of nlsGFP+ cells.

Quantification of GFP and mCherry expression, stereomicroscopy
For quantification of GFP and mCherry expression post lesion the larvae were anesthetized with 0.02% Tricaine (MS222) and again embedded in 1% LMA in a glass bottom dish. The larvae were imaged once with an Andor Dragonfly Spinning Disk equipped with a sCMOS camera. For each time point a different set of larvae was used. Identical settings for magnification, exposure time, pinhole size, laser power and z-stack interval were used throughout the whole experiment. Quantification of intensity and cell number was performed with ImageJ software version 1.53c (measure, cell counter). The transgenic zebrafish line *osterix*:nGFP (*OlSp7*:nlsGFP^{zf132}) used in our studies carries a nuclear localization signal that is, however, inefficiently targeted to the nucleus (Knopf et al., 2011). Cells can be counted as individual entities as the signal between cells is not continuous, i.e. evident by reduced or missing

fluorescence. Macrophages were counted using the different planes of a z-stack, and the images presented in the figures represent the maximum projections of the respective z-stacks. The maximum projection was used for figures as the opercle is not entirely flat; it is rather bent and covers a z-range of roughly 60 μm. By way of using the individual z-planes, macrophages could be counted, even if they were crowded. In case we counted macrophages in time lapse movies: macrophages were counted in the maximum projection by reducing the frame/second rate of the movies. Due to their movement, this allowed their reliable identification.

Stereomicroscopy of fin fold resected zebrafish larvae and the head region of *ctsK*:nlsmCherry transgenic zebrafish, as well as of NFP-treated *osterix*: NTR-mCherry zebrafish, was performed using a Zeiss SteREO Discovery.V12 equipped with a AxioCam MRm and AxioVision software version 4.7.1.0.

Image processing
Brightness, contrast and levels were adjusted using Adobe Photoshop CS6 and 2020 software or Affinity Photo software. Images were processed with identical settings to adjust brightness and contrast for all experimental groups.

Statistical analysis
Statistical analysis was run using GraphPad Prism 8.3.1. Unpaired two-sided *t*-tests with Welch's correction, Tukey's multiple comparison one-way ANOVA and Sidak's multiple comparison two-way ANOVA tests were performed wherever applicable.

Author contributions
Conceptualization: K.G., F.K.; Methodology: K.G.; Formal analysis: K.G., A.C.L.-D., F.K.; Investigation: K.G., A.C.L.-D., A.D., A.K., F.K.; Writing - original draft: K.G., F.K.; Writing - review & editing: K.G., A.C.L.-D., F.K.; Visualization: K.G., A.C.L.-D., F.K.; Supervision: F.K.; Project administration: F.K.; Funding acquisition: F.K.

References
Ahmad, M., Hachemi, Y., Paxian, K., Mengele, F., Koenen, M. and Tuckermann, J. (2019). A jack of all trades: impact of glucocorticoids on cellular cross-talk in osteoimmunology. *Front. Immunol.* **10**, 2460. doi:10.3389/fimmu.2019.02460

Alexander, K. A., Chang, M. K., Maylin, E. R., Kohler, T., Müller, R., Wu, A. C., Van Rooijen, N., Sweet, M. J., Hume, D. A., Raggatt, L. J., et al. (2011). Osteal macrophages promote in vivo intramembranous bone healing in a mouse tibial injury model. *J. Bone Miner. Res.* **26**(7), 1517-1532. doi:10.1002/jbmr.354

Almeida, M. and O'Brien, C. A. (2013). Basic biology of skeletal aging: role of stress response pathways. *The J. Gerontol. Ser. A Biol. Sci. Med. Sci.* **68**, 1197-1208. doi:10.1093/gerona/glt079

Ando, K., Shibata, E., Hans, S., Brand, M. and Kawakami, A. (2017). Osteoblast production by reserved progenitor cells in zebrafish bone regeneration and maintenance. *Dev. Cell* **43**, 643-650.e3. doi:10.1016/j.devcel.2017.10.015

Andrew, J. G., Andrew, S. M., Freemont, A. J. and Marsh, D. R. (1994). Inflammatory cells in normal human fracture healing. *Acta Orthop. Scand.* **65**, 462-466. doi:10.3109/17453679408995493

Baek, K. H., Oh, K. W., Lee, W. Y., Lee, S. S., Kim, M. K., Kwon, H. S., Rhee, E. J., Han, J. H., Song, K. H., Cha, B. Y. et al. (2010). Association of oxidative stress with postmenopausal osteoporosis and the effects of hydrogen peroxide on osteoclast formation in human bone marrow cell cultures. *Calcif. Tissue Int.* **87**, 226-235. doi:10.1007/s00223-010-9393-9

Bai, X.-C., Lu, D., Liu, A., Zhang, Z., Li, X., Zou, Z., Zeng, W., Cheng, B. and Luo, S. (2005). Reactive oxygen species stimulates receptor activator of NF-κB ligand expression in osteoblast. *J. Biol. Chem.* **280**, 17497-17506. doi:10.1074/jbc.M409332200

Barros-Becker, F., Lam, P.-Y., Fisher, R. and Huttenlocher, A. (2017). Live imaging reveals distinct modes of neutrophil and macrophage migration within interstitial tissues. *J. Cell Sci.* **130**, 3801-3808. doi:10.1242/jcs.206128

Batoon, L., Millard, S. M., Wullschleger, M. E., Preda, C., Wu, A. C.-K., Kaur, S., Tseng, H.-W., Hume, D. A., Levesque, J.-P., Raggatt, L. J. et al. (2017). CD169+ macrophages are critical for osteoblast maintenance and promote intramembranous and endochondral ossification during bone repair. *Biomaterials* **196**, 51-66. doi:10.1016/j.biomaterials.2017.10.033

Bergemann, D., Massoz, L., Bourdouxhe, J., Carril Pardo, C. A., Voz, M. L., Peers, B. and Manfroid, I. (2018). Nifurpirinol: a more potent and reliable substrate compared to metronidazole for nitroreductase-mediated cell ablations. *Wound Repair. Regen.* **26**, 238-244. doi:10.1111/wrr.12633

Brand, M., Granato, M. and C, N.-V. (2002). Keeping and raising zebrafish. In *Zebrafish: A Practical Approach* (ed. C. Nuesslein-Volhard and R. Dahm), pp. 7-37. New York: Oxford University Press.

Brittijn, S. A., Duivesteijn, S. J., Belmamoune, M., Bertens, L. F. M., Bitter, W., Debruijn, J. D., Champagne, D. L., Cuppen, E., Flik, G., Vandenbroucke-Grauls, C. M. et al. (2009). Zebrafish development and regeneration: new tools for biomedical research. *Int. J. Dev. Biol.* **53**, 835-850. doi:10.1387/ijdb.082615sb

Cain, D. W. and Cidlowski, J. A. (2017). Immune regulation by glucocorticoids. *Nat. Rev. Immunol.* **17**, 233-247. doi:10.1038/nri.2017.1

Callaway, D. A. and Jiang, J. X. (2015). Reactive oxygen species and oxidative stress in osteoclastogenesis, skeletal aging and bone diseases. *J. Bone Miner. Metab.* **33**, 359-370. doi:10.1007/s00774-015-0656-4

Chatani, M., Takano, Y. and Kudo, A. (2011). Osteoclasts in bone modeling, as revealed by in vivo imaging, are essential for organogenesis in fish. *Dev. Biol.* **360**, 96-109. doi:10.1016/j.ydbio.2011.09.013

Chatzopoulou, A., Heijmans, J. P. M., Burgerhout, E., Oskam, N., Spaink, H. P., Meijer, A. H. and Schaaf, M. J. M. (2016). Glucocorticoid-induced attenuation of the inflammatory response in Zebrafish. *Endocrinology* **157**, 2772-2784. doi:10.1210/en.2015-2050

Chen, A. T. and Zon, L. I. (2009). Zebrafish blood stem cells. *J. Cell Biochem.* **108**, 35-42. doi:10.1002/jcb.22251

Colombelli, J., Grill, S. W. and Stelzer, E. H. K. (2004). Ultraviolet diffraction limited nanosurgery of live biological tissues. *Rev. Sci. Instrum.* **75**, 472-478. doi:10.1063/1.1641163

Cox, B. D., De Simone, A., Tornini, V. A., Singh, S. P., Di Talia, S. and Poss, K. D. (2018). In toto imaging of dynamic osteoblast behaviors in regenerating skeletal bone. *Curr. Biol.* **28**, 3937-3947.e4. doi:10.1016/j.cub.2018.10.052

Cubbage, C. C. and Mabee, P. M. (1996). Development of the cranium and paired fins in the zebrafishDanio rerio (Ostariophysi, Cyprinidae). *J. Morphol.* **229**, 121-160. doi:10.1002/(SICI)1097-4687(199608)229:2<121::AID-JMOR1>3.0.CO;2-4

Curado, S., Stainier, D. Y. R. and Anderson, R. M. (2008). Nitroreductase-mediated cell/tissue ablation in zebrafish: a spatially and temporally controlled ablation method with applications in developmental and regeneration studies. *Nat. Protoc.* **3**, 948-954. doi:10.1038/nprot.2008.58

Dallas, S. L. and Moore, D. S. (2020). Using confocal imaging approaches to understand the structure and function of osteocytes and the lacunocanalicular network. *Bone* **138**, 115463. doi:10.1016/j.bone.2020.115463

Davies, L. C., Jenkins, S. J., Allen, J. E. and Taylor, P. R. (2013). Tissue-resident macrophages. *Nat. Immunol.* **14**, 986-995. doi:10.1038/ni.2705

De Simone, A., Evanitsky, M. N., Hayden, L., Cox, B. D., Wang, J., Tornini, V. A., Ou, J., Chao, A., Poss, K. D. and Di Talia, S. (2021). Control of osteoblast regeneration by a train of Erk activity waves. *Nature* **590**, 129. doi:10.1038/s41586-020-03085-8

Debnath, S., Yallowitz, A. R., Mccormick, J., Lalani, S., Zhang, T., Xu, R., Li, N., Liu, Y., Yang, Y. S., Eiseman, M. et al. (2018). Discovery of a periosteal stem cell mediating intramembranous bone formation. *Nature* **562**, 133-139. doi:10.1038/s41586-018-0554-8

Dehnisch Ellström, I., Spulber, S., Hultin, S., Norlin, N., Ceccatelli, S., Hultling, C. and Uhlén, P. (2019). Spinal cord injury in zebrafish induced by near-infrared femtosecond laser pulses. *J. Neurosci. Methods* **311**, 259-266. doi:10.1016/j.jneumeth.2018.10.035

Demy, D. L., Tauzin, M., Lancino, M., Le Cabec, V., Redd, M., Murayama, E., Maridonneau-Parini, I., Trede, N. and Herbomel, P. (2017). Trim33/Tif1-γ is essential for macrophage and neutrophil mobilisation to developmental or inflammatory cues. *J. Cell Sci.* **130**, 2797-2807. doi:10.1242/jcs.203471

Den Uyl, D., Bultink, I. E. M. and Lems, W. F. (2011). Glucocorticoid-induced osteoporosis. *Clin. Exp. Rheumatol.* **29** 5 Suppl. 68, S93-S98. Available at: http://www.ncbi.nlm.nih.gov/pubmed/22018192.

Diez-Roux, G. and Lang, R. A. (1997). Macrophages induce apoptosis in normal cells in vivo. *Development* **124**, 3633-3638. doi:10.1242/dev.124.18.3633

Duffield, J. S. (2003). The inflammatory macrophage: a story of Jekyll and Hyde. *Clin. Sci.* **104**, 27-38. doi:10.1042/CS20020240

Ellett, F., Pase, L., Hayman, J. W., Andrianopoulos, A. and Lieschke, G. J. (2011). mpeg1 promoter transgenes direct macrophage-lineage expression in zebrafish. *Blood* **117**, e49-e56. doi:10.1182/blood-2010-10-314120

Feng, X. and Mcdonald, J. M. (2011). Disorders of bone remodeling. *Annu. Rev. Pathol. Mech. Dis.* **6**, 121-145. doi:10.1146/annurev-pathol-011110-130203

Feng, Y., Santoriello, C., Mione, M., Hurlstone, A. and Martin, P. (2010). Live imaging of innate immune cell sensing of transformed cells in zebrafish larvae: parallels between tumor initiation and wound inflammation. *PLoS Biol.* **8**, e1000562. doi:10.1371/journal.pbio.1000562

Fiedler, I. A. K., Schmidt, F. N., Wölfel, E. M., Plumeyer, C., Milovanovic, P., Gioia, R., Tonelli, F., Bale, H. A., Jähn, K., Besio, R. et al. (2018). Severely impaired bone material quality in chihuahua zebrafish resembles classical dominant human osteogenesis imperfecta. *J. Bone Miner. Res.* **33**, 1489-1499. doi:10.1002/jbmr.3445

Formella, I., Svahn, A. J., Radford, R. A. W., Don, E. K., Cole, N. J., Hogan, A., Lee, A., Chung, R. S. and Morsch, M. (2018). Real-time visualization of oxidative stress-mediated neurodegeneration of individual spinal motor neurons in vivo. *Redox. Biol.* **19**, 226-234. doi:10.1016/j.redox.2018.08.011

Furuya, M., Kikuta, J., Fujimori, S., Seno, S., Maeda, H., Shirazaki, M., Uenaka, M., Mizuno, H., Iwamoto, Y., Morimoto, A. et al. (2018). Direct cell-cell contact between mature osteoblasts and osteoclasts dynamically controls their functions in vivo. *Nat. Commun.* **9**, 1-12. doi:10.1038/s41467-017-02541-w

Gauron, C., Rampon, C., Bouzaffour, M., Ipendey, E., Teillon, J., Volovitch, M. and Vriz, S. (2013). Sustained production of ROS triggers compensatory proliferation and is required for regeneration to proceed. *Sci. Rep.* **3**, 2084. doi:10.1038/srep02084

Geurtzen, K., Knopf, F., Wehner, D., Huitema, L. F. A., Schulte-Merker, S. and Weidinger, G. (2014). Mature osteoblasts dedifferentiate in response to traumatic bone injury in the zebrafish fin and skull. *Development* **141**, 2225-2234. doi:10.1242/dev.105817

Geurtzen, K., Vernet, A., Freidin, A., Rauner, M., Hofbauer, L. C., Schneider, J. E., Brand, M. and Knopf, F. (2017). Immune suppressive and bone inhibitory effects of prednisolone in growing and regenerating zebrafish tissues. *J. Bone Miner. Res.* **32**, 2476-2488. doi:10.1002/jbmr.3231

Gistelinck, C., Kwon, R. Y., Malfait, F., Symoens, S., Harris, M. P., Henke, K., Hawkins, M. B., Fisher, S., Sips, P., Guillemyn, B. et al. (2018). Zebrafish type I collagen mutants faithfully recapitulate human type I collagenopathies. *Proc. Natl. Acad. Sci. USA* **115**, E8037-E8046. doi:10.1073/pnas.1722200115

Gray, C., Loynes, C., Whyte, M., Crossman, D., Renshaw, S. and Chico, T. (2011). Simultaneous intravital imaging of macrophage and neutrophil behaviour during inflammation using a novel transgenic zebrafish. *Thromb. Haemostasis* **105**, 811-819. doi:10.1160/TH10-08-0525

Hall, C., Flores, M. V., Chien, A., Davidson, A., Crosier, K. and Crosier, P. (2009). Transgenic zebrafish reporter lines reveal conserved Toll-like receptor signaling potential in embryonic myeloid leukocytes and adult immune cell lineages. *J. Leukoc. Biol.* **85**, 751-765. doi:10.1189/jlb.0708405

Hall, C. J., Boyle, R. H., Sun, X., Wicker, S. M., Misa, J. P., Krissansen, G. W., Print, C. G., Crosier, K. E. and Crosier, P. S. (2014). Epidermal cells help coordinate leukocyte migration during inflammation through fatty acid-fuelled matrix metalloproteinase production. *Nat. Commun.* **5**, 3880. doi:10.1038/ncomms4880

Hammond, C. L. and Moro, E. (2012). Using transgenic reporters to visualize bone and cartilage signaling during development in vivo. *Front. Endocrinol.* **3**, 91. doi:10.3389/fendo.2012.00091

Hans, S., Kaslin, J., Freudenreich, D. and Brand, M. (2009). Temporally-controlled site-specific recombination in zebrafish. *PLoS ONE* **4**, e4640. doi:10.1371/journal.pone.0004640

Hasegawa, T., Hall, C. J., Crosier, P. S., Abe, G., Kawakami, K., Kudo, A. and Kawakami, A. (2017). Transient inflammatory response mediated by interleukin-1β is required for proper regeneration in zebrafish fin fold. *eLife* **6**, e22716. doi:10.7554/eLife.22716

Hasegawa, T., Kikuta, J. and Ishii, M. (2019). Imaging the bone-immune cell interaction in bone destruction. *Front. Immunol.* **10**, 596. doi:10.3389/fimmu.2019.00596

Hayes, A. J., Reynolds, S., Nowell, M. A., Meakin, L. B., Habicher, J., Ledin, J., Bashford, A., Caterson, B. and Hammond, C. L. (2013). Spinal deformity in aged zebrafish is accompanied by degenerative changes to their vertebrae that resemble osteoarthritis. *PLoS ONE* **8**, e75787. doi:10.1371/journal.pone.0075787

Hess, I. and Boehm, T. (2012). Intravital imaging of thymopoiesis reveals dynamic lympho-epithelial interactions. *Immunity* **36**, 298-309. doi:10.1016/j.immuni.2011.12.016

Huang, C., Ness, V. P., Yang, X., Chen, H., Luo, J., Brown, E. B. and Zhang, X. (2015). Spatiotemporal analyses of osteogenesis and angiogenesis via intravital imaging in cranial bone defect repair. *J. Bone Miner. Res.* **30**, 1217-1230. doi:10.1002/jbmr.2460

Ishii, M., Egen, J. G., Klauschen, F., Meier-Schellersheim, M., Saeki, Y., Vacher, J., Proia, R. L. and Germain, R. N. (2009). Sphingosine-1-phosphate mobilizes osteoclast precursors and regulates bone homeostasis. *Nature* **458**, 524-528. doi:10.1038/nature07713

Isles, H. M., Herman, K. D., Robertson, A. L., Loynes, C. A., Prince, L. R., Elks, P. M. and Renshaw, S. A. (2019). The CXCL12/CXCR4 signaling axis retains neutrophils at inflammatory sites in zebrafish. *Front. Immunol.* **10**, 1784. doi:10.3389/fimmu.2019.01784

Javidan, Y. and Schilling, T. F. (2004). Development of cartilage and bone. *Methods Cell Biol.* **76**, 415-436. doi:10.1016/S0091-679X(04)76018-5

Jelcic, M., Enyedi, B., Xavier, J. B. and Niethammer, P. (2017). Image-based measurement of H2O2 reaction-diffusion in wounded Zebrafish Larvae. *Biophys. J.* **112**, 2011-2018. doi:10.1016/j.bpj.2017.03.021

Jilka, R. L., Weinstein, R. S., Parfitt, A. M. and Manolagas, S. C. (2007). Perspective: quantifying osteoblast and osteocyte apoptosis: challenges and rewards. *J. Bone Miner. Res.* **22**, 1492-1501. doi:10.1359/jbmr.070518

Kaufmann, A., Mickoleit, M., Weber, M. and Huisken, J. (2012). Multilayer mounting enables long-term imaging of zebrafish development in a light sheet microscope. *Development (Camb.)* **139**, 3242-3247. doi:10.1242/dev.082586

Keightley, M.-C., Wang, C.-H., Pazhakh, V. and Lieschke, G. J. (2014). Delineating the roles of neutrophils and macrophages in zebrafish regeneration models. *Int. J. Biochem. Cell Biol.* **56**, 92-106. doi:10.1016/j.biocel.2014.07.010

Kennedy, O. D., Herman, B. C., Laudier, D. M., Majeska, R. J., Sun, H. B. and Schaffler, M. B. (2012). Activation of resorption in fatigue-loaded bone involves both apoptosis and active pro-osteoclastogenic signaling by distinct osteocyte populations. *Bone* **50**, 1115-1122. doi:10.1016/j.bone.2012.01.025

Kikuta, J., Kawamura, S., Okiji, F., Shirazaki, M., Sakai, S., Saito, H. and Ishii, M. (2013). Sphingosine-1-phosphate-mediated osteoclast precursor monocyte migration is a critical point of control in antibone-resorptive action of active vitamin D. *Proc. Natl. Acad. Sci. USA* **110**, 7009-7013. doi:10.1073/pnas.1218799110

Kim, J. M. and Bixel, M. G. (2020). Intravital multiphoton imaging of the bone and bone marrow environment. *Cytometry Part A* **97**, 496-503. doi:10.1002/cyto.a.23937

Kim, H.-N., Iyer, S., Ring, R. and Almeida, M. (2018). The role of FoxOs in bone health and disease. *Curr. Top. Dev. Biol.* **127**, 149-163. doi:10.1016/bs.ctdb.2017.10.004

Kimmel, C. B., Delaurier, A., Ullmann, B., Dowd, J. and Mcfadden, M. (2010). Modes of developmental outgrowth and shaping of a craniofacial bone in zebrafish. *PLoS ONE* **5**, e9475-e9475. doi:10.1371/journal.pone.0009475

Knopf, F., Hammond, C., Chekuru, A., Kurth, T., Hans, S., Weber, C. W., Mahatma, G., Fisher, S., Brand, M., Schulte-Merker, S. et al. (2011). Bone regenerates via dedifferentiation of osteoblasts in the Zebrafish Fin. *Dev. Cell* **20**, 713-724. doi:10.1016/j.devcel.2011.04.014

Kolaczkowska, E. and Kubes, P. (2013). Neutrophil recruitment and function in health and inflammation. *Nat. Rev. Immunol.* **13**, 159-175. doi:10.1038/nri3399

Kulkarni, A. A., Conteh, A. M., Sorrell, C. A., Mirmira, A., Tersey, S. A., Mirmira, R. G., Linnemann, A. K. and Anderson, R. M. (2018). An in vivo zebrafish model for interrogating ROS-mediated pancreatic β-cell injury, response, and prevention. *Oxid. Med. Cell. Longevity* **2018**, 1324739. doi:10.1155/2018/1324739

Lean, J. M., Jagger, C. J., Kirstein, B., Fuller, K. and Chambers, T. J. (2005). Hydrogen peroxide is essential for estrogen-deficiency bone loss and osteoclast formation. *Endocrinology* **146**, 728-735. doi:10.1210/en.2004-1021

LeBert, D. C., Squirrell, J. M., Rindy, J., Broadbridge, E., Lui, Y., Zakrzewska, A., Eliceiri, K. W., Meijer, A. H. and Huttenlocher, A. (2015). Matrix metalloproteinase 9 modulates collagen matrices and wound repair. *Development (Camb.)* **142**, 2136-2146. doi:10.1242/dev.121160

Lee, N. K., Choi, Y. G., Baik, J. Y., Han, S. Y., Jeong, D.-, Bae, Y. S., Kim, N. and Lee, S. Y. (2005). A crucial role for reactive oxygen species in RANKL-induced osteoclast differentiation. *Blood* **106**, 852-859. doi:10.1182/blood-2004-09-3662

Leibovich, S. J. and Ross, R. (1975). The role of the macrophage in wound repair. A study with hydrocortisone and antimacrophage serum. *Am. J. Pathol.* **78**, 71-100.

Li, L., Yan, B., Shi, Y.-Q., Zhang, W.-Q. and Wen, Z.-L. (2012). Live imaging reveals differing roles of macrophages and neutrophils during zebrafish tail fin regeneration. *J. Biol. Chem.* **287**, 25353-25360. doi:10.1074/jbc.M112.349126

Lieschke, G. J., Oates, A. C., Crowhurst, M. O., Ward, A. C. and Layton, J. E. (2001). Morphologic and functional characterization of granulocytes and macrophages in embryonic and adult zebrafish. *Blood* **98**, 3087-3096. doi:10.1182/blood.V98.10.3087

Manolagas, S. C. (2000). Birth and death of bone cells: basic regulatory mechanisms and implications for the pathogenesis and treatment of osteoporosis. *Endocr. Rev.* **21**, 115-137. doi:10.1210/edrv.21.2.0395

Marjoram, L., Alvers, A., Deerhake, M. E., Bagwell, J., Mankiewicz, J., Cocchiaro, J. L., Beerman, R. W., Willer, J., Sumigray, K. D., Katsanis, N. et al. (2015). Epigenetic control of intestinal barrier function and inflammation in zebrafish. *Proc. Natl. Acad. Sci. USA* **112**, 2770-2775. doi:10.1073/pnas.1424089112

Mathias, J. R., Perrin, B. J., Liu, T.-X., Kanki, J., Look, A. T. and Huttenlocher, A. (2006). Resolution of inflammation by retrograde chemotaxis of neutrophils in transgenic zebrafish. *J. Leukoc. Biol.* **80**, 1281-1288. doi:10.1189/jlb.0506346

McDonald, G. L. K., Wang, M., Hammond, C. L. and Bergen, D. J. M. (2021). Pharmacological manipulation of early zebrafish skeletal development shows an important role for Smad9 in control of skeletal progenitor populations. *Biomolecules* **11**, 277. doi:10.3390/biom11020277

McWhorter, F. Y., Wang, T., Nguyen, P., Chung, T. and Liu, W. F. (2013). Modulation of macrophage phenotype by cell shape. *Proc. Natl. Acad. Sci. USA* **110**, 17253-17258. doi:10.1073/pnas.1308887110

Morsch, M., Radford, R. A. W., Don, E. K., Lee, A., Hortle, E., Cole, N. J. and Chung, R. S. (2017). Triggering cell stress and death using conventional UV laser confocal microscopy. *J. Vis. Exp.* **2017**. doi:10.3791/54983

Mosser, D. M. and Edwards, J. P. (2008). Exploring the full spectrum of macrophage activation. *Nat. Rev. Immunol.* **8**, 958-969. doi:10.1038/nri2448

Nguyen-Chi, M., Laplace-Builhe, B., Travnickova, J., Luz-Crawford, P., Tejedor, G., Phan, Q. T., Duroux-Richard, I., Levraud, J.-P., Kissa, K., Lutfalla, G. et al. (2015). Identification of polarized macrophage subsets in zebrafish. *eLife* **4**, e07288. doi:10.7554/eLife.07288

Nguyen-Chi, M., Laplace-Builhé, B., Travnickova, J., Luz-Crawford, P., Tejedor, G., Lutfalla, G., Kissa, K., Jorgensen, C. and Djouad, F. (2017). TNF signaling and macrophages govern fin regeneration in zebrafish larvae. *Cell Death Dis.* **8**, e2979. doi:10.1038/cddis.2017.374

Niethammer, P., Grabher, C., Look, A. T. and Mitchison, T. J. (2009). A tissue-scale gradient of hydrogen peroxide mediates rapid wound detection in zebrafish. *Nature* **459**, 996-999. doi:10.1038/nature08119

Novak, M. L. and Koh, T. J. (2013). Macrophage phenotypes during tissue repair. *J. Leukoc. Biol.* **93**, 875-881. doi:10.1189/jlb.1012512

O'Brien, G. S., Rieger, S., Wang, F., Smolen, G. A., Gonzalez, R. E., Buchanan, J. A. and Sagasti, A. (2012). Coordinate development of skin cells and cutaneous sensory axons in zebrafish. *J. Comp. Neurol.* **520**, 816-831. doi:10.1002/cne.22791

Odén, A., Mccloskey, E. V., Kanis, J. A., Harvey, N. C. and Johansson, H. (2015). Burden of high fracture probability worldwide: secular increases 2010–2040. *Osteoporos. Int.* **26**, 2243-2248. doi:10.1007/s00198-015-3154-6

Ohgo, S., Ichinose, S., Yokota, H., Sato-Maeda, M., Shoji, W. and Wada, N. (2019). Tissue regeneration during lower jaw restoration in zebrafish shows some features of epimorphic regeneration. *Dev. Growth Differ.* **61**, 419-430. doi:10.1111/dgd.12625

Ohnmacht, J., Yang, Y., Maurer, G. W., Barreiro-Iglesias, A., Tsarouchas, T. M., Wehner, D., Sieger, D., Becker, C. G. and Becker, T. (2016). Spinal motor neurons are regenerated after mechanical lesion and genetic ablation in larval zebrafish. *Development (Camb.)* **143**, 1464-1474. doi:10.1242/dev.129155

Paul, S., Schindler, S., Giovannone, D., De Millo Terrazzani, A., Mariani, F. V. and Crump, J. G. (2016). Ihha induces hybrid cartilage-bone cells during zebrafish jawbone regeneration. *Development* **143**, 2066-2076. doi:10.1242/dev.131292

Peti-Peterdi, J., Kidokoro, K. and Riquier-Brison, A. (2016). Intravital imaging in the kidney. *Curr. Opin Nephrol. Hypertens.* **25**, 168-173. doi:10.1097/MNH.0000000000000219

Petrie, T. A., Strand, N. S., Tsung-Yang, C., Rabinowitz, J. S. and Moon, R. T. (2014). Macrophages modulate adult zebrafish tail fin regeneration. *Development* **141**, 2581-2591. doi:10.1242/dev.098459

Pettit, A. R., Chang, M. K., Hume, D. A. and Raggatt, L.-J. (2008). Osteal macrophages: a new twist on coupling during bone dynamics. *Bone* **43**, 976-982. doi:10.1016/j.bone.2008.08.128

Phan, Q. T., Tan, W. H., Liu, R., Sundaram, S., Buettner, A., Kneitz, S., Cheong, B., Vyas, H., Mathavan, S., Schartl, M. et al. (2020a). Cxcl9l and Cxcr3.2 regulate recruitment of osteoclast progenitors to bone matrix in a medaka osteoporosis model. *Proc. Natl. Acad. Sci. USA* **117**, 19276-19286. doi:10.1073/pnas.2006093117

Phan, Q. T., Liu, R., Tan, W. H., Imangali, N., Cheong, B., Schartl, M. and Winkler, C. (2020b). Macrophages switch to an osteo-modulatory profile upon RANKL Induction in a Medaka (Oryzias latipes) Osteoporosis Model. *JBMR Plus* **4**, e10409. doi:10.1002/jbm4.10409

Purwar, R., Kraus, M., Werfel, T. and Wittmann, M. (2008). Modulation of keratinocyte-derived MMP-9 by IL-13: a possible role for the pathogenesis of epidermal inflammation. *J. Investig. Dermatol.* **128**, 59-66. doi:10.1038/sj.jid.5700940

Quinn, J. M. W., Neale, S., Fujikawa, Y. and Mcgee, J. O. D. (1998). Human osteoclast formation from blood monocytes, peritoneal macrophages, and bone marrow cells. *Calcif. Tissue Int.* **62**, 527-531. doi:10.1007/s002239900473

DEVELOPMENT

Renshaw, S. A. and Trede, N. S. (2012). A model 450 million years in the making: zebrafish and vertebrate immunity. *Dis. Model. Mech.* **5**, 38-47. doi:10.1242/dmm. 007138

Renshaw, S. A., Loynes, C. A., Trushell, D. M. I., Elworthy, S., Ingham, P. W. and Whyte, M. K. B. (2006). A transgenic zebrafish model of neutrophilic inflammation. *Blood* **108**, 3976-3978. doi:10.1182/blood-2006-05-024075

Renvoizé, C., Biola, A., Pallardy, M. and Bréard, J. (1998). Apoptosis: identification of dying cells. *Cell Biol. Toxicol.* **14**, 111-120. doi:10.1023/A:1007429904664

Robertson, A. L., Ogryzko, N. V., Henry, K. M., Loynes, C. A., Foulkes, M. J., Meloni, M. M., Wang, X., Ford, C., Jackson, M., Ingham, P. W. et al. (2016). Identification of benzopyrone as a common structural feature in compounds with anti-inflammatory activity in a zebrafish phenotypic screen. *Dis. Model. Mech.* **9**, 621-632. doi:10.1242/dmm.024935

Robinson, J. M. (2008). Reactive oxygen species in phagocytic leukocytes. *Histochem. Cell Biol.* **130**, 281-297. doi:10.1007/s00418-008-0461-4

Roger, R., Issaad, C., Pallardy, M., Leglise, M. C., Turhan, A. G., Bertoglio, J. and Breard, J. (1996). BCR-ABL does not prevent apoptotic death induced by human natural killer or lymphokine-activated killer cells. *Blood* **87**, 1113-1122. doi:10.1182/blood.V87.3.1113.bloodjournal8731113

Romero, M. M. G., McCathie, G., Jankun, P. and Roehl, H. H. (2018). Damage-induced reactive oxygen species enable zebrafish tail regeneration by repositioning of Hedgehog expressing cells. *Nat. Commun.* **9**, 4010. doi:10.1038/s41467-018-06460-2

Russo-Marie, F. (1992). Macrophages and the glucocorticoids. *J. Neuroimmunol.* **40**, 281-286. doi:10.1016/0165-5728(92)90144-A

Sanderson, L. E., Chien, A.-T., Astin, J. W., Crosier, K. E., Crosier, P. S. and Hall, C. J. (2015). An inducible transgene reports activation of macrophages in live zebrafish larvae. *Dev. Comp. Immunol.* **53**, 63-69. doi:10.1016/j.dci.2015.06.013

Serowoky, M. A., Arata, C. E., Crump, J. G. and Mariani, F. V. (2020). Skeletal stem cells: Insights into maintaining and regenerating the skeleton. *Development (Camb.)* **147**, dev179325. doi:10.1242/dev.179325

Sharif, F., De Bakker, M. A. G. and Richardson, M. K. (2014). Osteoclast-like cells in early zebrafish embryos. *Cell J.* **16**, 211-224. Available at: http://www.ncbi.nlm. nih.gov/pubmed/24567948.

Sharif, F., Steenbergen, P. J., Metz, J. R. and Champagne, D. L. (2015). Long-lasting effects of dexamethasone on immune cells and wound healing in the zebrafish. *Wound Repair. Regen.* **23**, 855-865. doi:10.1111/wrr.12366

Shiflett, L. A., Tiede-Lewis, L. A. M., Xie, Y., Lu, Y., Ray, E. C. and Dallas, S. L. (2019). Collagen dynamics during the process of osteocyte embedding and mineralization. *Front. Cell Dev. Biol.* **7**, 178. doi:10.3389/fcell.2019.00178

Sinder, B. P., Pettit, A. R. and Mccauley, L. K. (2015). Macrophages: their emerging roles in bone. *J. Bone Miner. Res.* **30**, 2140-2149. doi:10.1002/jbmr. 2735

Singh, S. P., Holdway, J. E. and Poss, K. D. (2012). Regeneration of amputated zebrafish fin rays from de novo osteoblasts. *Dev. Cell* **22**, 879-886. doi:10.1016/j. devcel.2012.03.006

Sousa, S., Afonso, N., Bensimon-Brito, A., Fonseca, M., Simões, M., Leon, J., Roehl, H., Cancela, M. L. and Jacinto, A. (2011). Differentiated skeletal cells contribute to blastema formation during zebrafish fin regeneration. *Development* **138**, 3897-3905. doi:10.1242/dev.064717

Spoorendonk, K. M., Peterson-Maduro, J., Renn, J., Trowe, T., Kranenbarg, S., Winkler, C. and Schulte-Merker, S. (2008). Retinoic acid and Cyp26b1 are critical regulators of osteogenesis in the axial skeleton. *Development* **135**, 3765-3774. doi:10.1242/dev.024034

Sugiyama, M., Sakaue-Sawano, A., Iimura, T., Fukami, K., Kitaguchi, T., Kawakami, K., Okamoto, H., Higashijima, S.- and Miyawaki, A. (2009). Illuminating cell-cycle progression in the developing zebrafish embryo. *Proc. Natl Acad. Sci. USA* **106**, 20812-20817. doi:10.1073/pnas.0906464106

Takayanagi, H. (2007). Osteoimmunology: shared mechanisms and crosstalk between the immune and bone systems. *Nat. Rev. Immunol.* **7**, 292-304. doi:10. 1038/nri2062

Tan, H.-Y., Wang, N., Li, S., Hong, M., Wang, X. and Feng, Y. (2016). The reactive oxygen species in macrophage polarization: reflecting its dual role in progression and treatment of human diseases. *Oxid. Med. Cell. Longevity* **2016**, 2795090. doi:10.1155/2016/2795090

Teh, C., Chudakov, D. M., Poon, K.-L., Mamedov, I. Z., Sek, J.-Y., Shidlovsky, K., Lukyanov, S. and Korzh, V. (2010). Optogenetic in vivo cell manipulation in KillerRed-expressing zebrafish transgenics. *BMC Dev. Biol.* **10**, 110. doi:10.1186/1471-213X-10-110

Tonelli, F., Cotti, S., Leoni, L., Besio, R., Gioia, R., Marchese, L., Giorgetti, S., Villani, S., Gistelinck, C., Wagener, R. et al. (2020). Crtap and p3h1 knock out zebrafish support defective collagen chaperoning as the cause of their osteogenesis imperfecta phenotype. *Matrix Biol.* **90**, 40-60. doi:10.1016/j.matbio.2020.03.004

Trede, N. S., Langenau, D. M., Traver, D., Look, A. T. and Zon, L. I. (2004). The use of zebrafish to understand immunity. *Immunity* **20**, 367-379. doi:10.1016/S1074-7613(04)00084-6

Walton, E. M., Cronan, M. R., Beerman, R. W. and Tobin, D. M. (2015). The macrophage-specific promoter mfap4 allows live, long-term analysis of macrophage behavior during mycobacterial infection in Zebrafish. *PLoS ONE* **10**, e0138949. doi:10.1371/journal.pone.0138949

Weinstein, R. S. (2012). Glucocorticoid-induced osteoporosis and osteonecrosis. *Endocrinol. Metab. Clin. N. Am.* **41**, 595-611. doi:10.1016/j.ecl.2012.04.004

Witten, P. E. and Huysseune, A. (2009). A comparative view on mechanisms and functions of skeletal remodelling in teleost fish, with special emphasis on osteoclasts and their function. *Biol. Rev.* **84**, 315-346. doi:10.1111/j.1469-185X. 2009.00077.x

Woodfin, A., Voisin, M.-B., Beyrau, M., Colom, B., Caille, D., Diapouli, F.-M., Nash, G. B., Chavakis, T., Albelda, S. M., Rainger, G. E. et al. (2011). The junctional adhesion molecule JAM-C regulates polarized transendothelial migration of neutrophils in vivo. *Nat. Immunol.* **12**, 761-769. doi:10.1038/ni.2062

Xie, Y., Tolmeijer, S., Oskam, J. M., Tonkens, T., Meijer, A. H. and Schaaf, M. J. M. (2019). Glucocorticoids inhibit macrophage differentiation towards a pro-inflammatory phenotype upon wounding without affecting their migration. *Dis. Model. Mech.* **12**, dmm037887. doi:10.1242/dmm.037887

Yang, Y., Hippensteel, J. A. and Schmidt, E. P. (2018). Intravital microscopy in the mouse lung. *Methods Mol. Biol.* **1809**, 331-339. doi:10.1007/978-1-4939-8570-8_21

Yoo, S. K., Freisinger, C. M., Lebert, D. C. and Huttenlocher, A. (2012). Early redox, Src family kinase, and calcium signaling integrate wound responses and tissue regeneration in zebrafish. *J. Cell Biol.* **199**, 225-234. doi:10.1083/jcb. 201203154

DEVELOPMENT